Title page

PTEN neddylation aggravates CDK4/6 inhibitor resistance in breast cancer

Fan Liu [1,2]†, Weixiao Liu [1,2]†, Yawen Tan [3]†, Yaxin Shang [1], Sihui Ling [1], Xiaokun Jiang [4], Zhen Zhang [4], Shiyao Sun [3], Ping Xie [1,2*]

1 Department of Cell Biology, Beijing Key Laboratory of Cancer Invasion and Metastasis Research, Capital Medical University, Beijing 100069, China.

2 Beijing lnstitute of Hepatology, Beijing Youan Hospital, Capital Medical University, Beijing 100069, China.

3 Department of Breast and Thyroid Surgery, The Second People's Hospital of Shenzhen, Shenzhen, Guangdong 518035, China.

4 Department of Neurosurgery, Shandong Provincial Hospital affiliated to Shandong First Medical University, Jinan, Shandong 250021, China.

*Correspondence: Ping Xie (xiep@ccmu.edu.cn).

† These authors contributed equally to this work: Fan Liu, Weixiao Liu, Yawen Tan.

PTEN neddylation aggravates CDK4/6 inhibitor resistance in breast cancer

Fan Liu [1,2]†, Weixiao Liu [1,2]†, Yawen Tan [3]†, Yaxin Shang [1], Sihui Ling [1], Xiaokun Jiang [4], Zhen Zhang [4], Shiyao Sun [3], Ping Xie [1,2*]

1 Department of Cell Biology, Beijing Key Laboratory of Cancer Invasion and Metastasis Research, Capital Medical University, Beijing 100069, China.

2 Beijing lnstitute of Hepatology, Beijing Youan Hospital, Capital Medical University, Beijing 100069, China.

3 Department of Breast and Thyroid Surgery, The Second People's Hospital of Shenzhen, Shenzhen, Guangdong 518035, China.

4 Department of Neurosurgery, Shandong Provincial Hospital affiliated to Shandong First Medical University, Jinan, Shandong 250021, China.

*Correspondence: Ping Xie (xiep@ccmu.edu.cn).

† These authors contributed equally to this work: Fan Liu, Weixiao Liu, Yawen Tan.

Abstract

Background: The gradual emergence of a novel therapeutic approach lies in the restoration of tumor suppressive machinery. PTEN is a crucial negative regulator of the PI3K/Akt signaling pathway. Protein neddylation modification contributes to PTEN inactivation and fuels breast cancer progression.

Methods: In this study, well-established CDK4/6 inhibitor resistance models were used to detect the levels of PTEN neddylation. Co-immunoprecipitation, *in vivo* and *in vitro* modification assays and transcriptome data were integrated to delve into the mechanism. Following this, a PTEN neddylation inhibitor identified through virtual screening was shown to overcome resistance to

CDK4/6 inhibitors in both *in situ* tumor models and breast cancer cells. Furthermore, in patient-derived organoids (PDOs), we combined the PTEN neddylation inhibitor with CDK4/6 inhibitors to confirm their inhibitory effect on breast cancer progression.

Results: We highlight that an elevated level of PTEN neddylation is markedly associated with resistance to palbociclib, a CDK4/6 inhibitor used in luminal subtype breast cancer patients. Mechanistically, PTEN neddylation activates the PI3K/Akt signaling pathway, and more notably, upregulates the activity of the AP-1 transcription factor. Our data showed that PTEN neddylation stabilizes JUND, a transcription factor involved in the AP-1, by disrupting its interaction with the E3 ubiquitin ligase ITCH. Consequently, activated JUND leads to the release of cytokines and chemokines, such as G-CSF, GM-CSF, IL-1RA, IL-1β, which in turn may drive an inflammatory tumor microenvironment, potentially contributing to drug resistance. Then, we identified Echinacoside as a potent inhibitor of PTEN neddylation both *in vivo* and *in vitro* by disrupting its interaction with XIAP, the E3 ligase responsible for PTEN neddylation. Combination of Echinacoside could effectively overcome resistance to palbociclib in breast cancer treatment.

Conclusions: This novel insight underscores the potential of targeting PTEN neddylation as a promising strategy for restoring the activity of key tumor suppressor and overcoming resistance in breast cancer therapy.

Keywords: breast cancer, CDK4/6 inhibitor resistance, JUND, neddylation, PTEN

Background

Breast cancer is a heterogeneous disease with multiple intrinsic tumor subtypes. The luminal breast cancer subtype, characterized by the expression of hormone receptor-positive (HR+) and human epidermal growth factor receptor 2-negative (HER2-) accounts for 70 % of breast cancer patients [1, 2]. Cyclin D-dependent Kinases 4 and 6 inhibitors (CDK4/6i) have been approved by the FDA for the treatment of luminal breast cancer [3-5]. Although patients with advanced disease have benefited from CDK4/6 inhibitors, drug resistance still remains a significant clinical challenge [6-

8]. Many factors contribute to CDK4/6i resistance, including CDK4/6 and Cyclin D1 overexpression, p16 amplification, loss of p53, loss of retinoblastoma (Rb) and over-activation of CDK2. Notably, resistance to CDK4/6 inhibitors is also prominently characterized by over-activated PI3K/Akt signaling pathway [9-13]. However, although PI3K inhibitors could prevent resistance to CDK4/6 inhibitors, they failed to re-sensitize cells once resistance had been acquired [14, 15]. PTEN (phosphatase and tension homologue deleted from chromosome 10) is a well-known negative regulator of the PI3K signaling pathway and governs fundamental cellular processes [16-19]. Recently, PTEN loss is considered as a bona fide mechanism of resistance to CDK4/6 inhibitors. Loss of PTEN increases PI3K/Akt activity and increases activity of CDK4/6 [20-22]. Therefore, targeting the restoration of PTEN tumor suppressor activity is believed to be a more effective approach in tumor treatment [23, 24].

Nedd8, a ubiquitin-like protein covalently conjugated to substrates similar to ubiquitin, mediates protein post-translational modification called neddylation [25]. Neddylation involves the covalent attachment of Nedd8 to a substrate through an ATP-dependent cascade involving the Nedd8-activating enzyme (E1, UBA3/APPBP1), Nedd8-conjugating enzyme (E2, UBE2M and UBE2F), and Nedd8 ligases (E3). The substrates of neddylation include both cullin proteins and non-cullin proteins [26, 27]. Over-active neddylation modification has been indicated to be closely correlated with cancer development. The first-in-class neddylation E1 inhibitor, MLN4924 (pevonedistat), has entered in several phases of clinical trials for tumor therapy [28]. Additionally, several inhibitors targeting E2s have shown well anti-tumor activity in mice models [29]. Up to now, none of them is granted by FDA for the treatment of cancer. It's still necessary to discover more potent and selective neddylation inhibitors for clinical trials. Our previous study found that high levels of PTEN neddylation, which lead to PTEN inactivation, enhance the activity of the PI3K/Akt pathway, promote PTEN nuclear import, and accelerate breast tumor proliferation and invasion [30, 31]. Here, we found that PTEN neddylation is elevated in luminal-type breast cancer patients with resistance

96 to palbociclib by promoting JUND protein stability and AP-1 transcriptional activation.
97 Furthermore, we proposed that Echinacoside (ECH), a natural phenylethanoid glycoside in
98 *Echinacea angustifolia* DC, acts as a potent PTEN neddylation inhibitor. Combined treatment of
99 ECH therapeutically blunted palbociclib resistance and enhanced drug sensitivity. Therefore, we
100 provide an innovative therapeutic strategy to limit cancer drug resistance through PTEN
101 reactivation by blocking neddylation modification.

102 **Methods**

103 **Patients and mice**

104 The clinical samples were approved by the department of breast and thyroid surgery at the Second
105 People's Hospital of Shenzhen and Hunan Cancer Hospital. Informed consent was obtained from
106 all subjects or their relatives. The MMTV-*PyMT* mice (*PyMT*/WT mice, background C57BL/6J
107 (RRID: IMSR_JAX: 000664)) were purchased from Cyagen Biosciences. CD-1(ICR, RRID:
108 IMSR_CRL: 022) mice were purchased from Beijing Vital River Laboratory Animal Technology
109 Co., Ltd. Animals were assigned to experimental groups using simple randomization.

110 **Cell culture and reagents**

111 All mammalian cells were cultured following ATCC recommended protocols and in medium
112 supplemented with 10 % fetal bovine serum (FBS, VivaCell BIOSCIENCES C04001-500) and 1 %
113 penicillin-streptomycin (Gene-Protien Link P08X14). MCF-7 (RRID: CVCL_0031), HEK293T
114 (RRID: CVCL_0063), HCT116 (RRID: CVCL_0291), A549 (RRID: CVCL_0023), MDA-MB-
115 231 (RRID: CVCL_0062), MCF-7 sh*PTEN*, MCF-7 sh*PTEN*+PTEN-Nedd8, MCF-7
116 sh*PTEN*+NLS-PTEN, MCF-7 sh*PTEN*+PTEN-WT and MCF-7 sh*PTEN*+PTEN-2KR cells were
117 cultured in Dulbecco's modified Eagle's medium (DMEM) with high glucose (Thermo Fisher
118 Scientific). T-47D (RRID: CVCL_0553) and T98G (RRID: CVCL_0556) cells were cultured in
119 RPMI-1640 medium (Thermo Fisher Scientific). MCF-7 sublines resistant to doxorubicin (MCF-
120 7/ADR) were purchased from Sunncell Biosciences and were cultured in RPMI-1640 medium
121 supplemented with 500 ng/ml doxorubicin hydrochloride. MCF-7 sublines resistant to cisplatin

122 (MCF-7/DDP) were purchased from Shanghai Mei Xuan Biological Technology Co., Ltd and were
123 cultured in RPMI-1640 medium supplemented with 500 ng/ml cisplatin. MCF-7 sublines resistant
124 to paclitaxel (MCF-7/PTX) were purchased from BLUEFBIO (Shanghai, China) and were cultured
125 in Dulbecco's modified Eagle's medium (DMEM) with high glucose supplemented with 200 ng/ml
126 paclitaxel. All cell lines were authenticated by STR profiling.
127 Palbociclib (HY-50767), Pevonedistat (HY-70062), Echinacoside (HY-N0020), Maltotetraose (HY-
128 N2464), MG132 (HY-13259), Cisplatin (HY-17394), Paclitaxel (HY-B0015), Doxorubicin
129 hydrochloride (HY-15142), Z21911837, Z45457765 and Z1549417413 were purchased from *Med*
130 *Chem Express*.

131 **Establishment of palbociclib-resistant cells**

132 To generate the palbociclib-resistant cells, the cells were cultured in media supplemented with
133 increasing concentrations of palbociclib for over 6 months. The concentration of palbociclib were
134 began at 100 nmol/L and were maintained at a final dose of 6 μmol/L. The palbociclib-resistant
135 cells were named as MCF-7-PR cells (MCF-7 palbociclib-resistant cells). For all experiments, the
136 resistant cells were refreshed with palbociclib-free media for 48 h before treatment.

137 **Antibodies**

138 The following antibodies were used: Phospho-Rb (Ser807/811) (Cat# 8516, RRID: AB_11178658),
139 Rb (Cat# 9309, RRID: AB_823629), Cyclin D1 (Cat# 2922, RRID: AB_2228523), PTEN (Cat#
140 9188, RRID: AB_2253290), Ubiquitin (Cat# 20326, RRID: AB_3064918), Akt (Cat# 9272, RRID:
141 AB_329827), Phospho-Akt (Ser473) (Cat# 9271, RRID: AB_329825), Phospho-Akt (Thr308)
142 (Cat# 13038, RRID: AB_2629447), Phospho-JUND (Ser100) (Cat# 9164, RRID: AB_330892),
143 CUL1 (Cat# 4995, RRID: AB_2261133), XIAP (Cat# 2042, RRID: AB_2214870), Nedd8 (Cat#
144 2754, RRID: AB_659972), c-JUN (Cat# 9165, RRID: AB_2130165), JUNB (Cat# 3753, RRID:
145 AB_2130002), c-FOS (Cat# 2250, RRID: AB_2247211) and FOSB (Cat# 2251, RRID:
146 AB_2106903) antibodies were purchased from Cell Signaling Technology. Ly6G (Cat# sc-53515,

147 RRID: AB_783639), CD3 (Cat# sc-18843, RRID: AB_627010), CD4 (Cat# sc-53042, RRID:
148 AB_629062), CD8 (Cat# sc-53063, RRID: AB_629231), CD11b (Cat# sc-1186, RRID:
149 AB_626884), NEDP1 (Cat# sc-271498, RRID: AB_10649498) and Cyclin E (Cat# sc-377100,
150 RRID: AB_2923122) antibodies were purchased from Santa Cruz Biotechnology. F4/80 (Cat#
151 28463-1-AP, RRID: AB_2881149), GAPDH (Cat# 60004-1-Ig, RRID: AB_2107436), UBA3 (Cat#
152 68067-1-Ig, RRID: AB_2918808), Ubc12 (Cat# CL488-67482, RRID: AB_3084351), ITCH
153 (Cat#20920-1-AP, RRID: AB_2878765) and GST (Cat# HRP-66001, RRID: AB_2883833)
154 antibodies were purchased from Proteintech. Flag (Cat# M185-3L, RRID: AB_11123930), Myc
155 (Cat# M047-3, RRID: AB_591112) and HA (Cat# M132-3, RRID: AB_10207271) antibodies were
156 purchased from MBL. JUND (Cat# A5433, RRID: AB_2863501) and FOSL1 (Cat# A5372, RRID:
157 AB_2766182) antibodies were purchased from ABclonal. Goat anti-Rabbit IgG (H + L) Secondary
158 Antibody (Cat# 65-6120, RRID: AB_2533967) and Goat anti-Mouse IgG (H + L) Secondary
159 Antibody (Cat# 31430, RRID: AB_228307) were purchased from Thermo Fisher Scientific. PTEN-
160 Nedd8 (K402) antibody was purchased from PTM BioLab (Hang Zhou) Co., Inc.

161 **Palbociclib-resistant Mice**

162 The palbociclib-sensitive MMTV-*PyMT* mice were obtained by continuing palbociclib (75 mg/kg)
163 gavage for 20 days. Palbociclib-resistant MMTV-*PyMT* mice were obtained by continuing
164 palbociclib (75 mg/kg) gavage for 35 days.

165 **RNA-seq Analysis**

166 Total RNA was extracted with TRIzol (Cat# 15596; Invitrogen) and the quality matched the
167 requirement of database sequencing. After that, RNA was digested for reverse transcription, and
168 rRNA was degraded. A complementary DNA library was prepared, and sequencing was performed
169 according to the Illumina standard protocol by Novogene Technology Co., Ltd. (Beijing, China).
170 Reads were normalized and fragments per kilobase per million mapped reads (FPKMs) were
171 calculated through RSEM. MA-plot-based method was used to filter differentially expressed genes

172 (DEGs), and genes with log2 ratio ⩾ 2 and *Q*-value ⩽ 0.001 were considered significantly
173 regulated. Gene ontology enrichment and Kyoto Encyclopedia of Genes and Genomes pathway
174 analysis of DEGs were performed using Phyper function in R software. FDR correction was
175 performed on *P*-value, and *Q*-value ⩽ 0.05 considered as significant enrichment.

176 **Immunoprecipitation and immunoblotting**

177 For immunoprecipitation assays, cells were lysed in EBC lysis buffer (0.5 % NP-40, 50 mM Tris,
178 pH 7.6, 120 mM NaCl, 1 mM EDTA, 1 mM Na_3VO_4, 50 mM NaF and 1 mM β-mercaptoethanol)
179 supplemented with protease inhibitor cocktail (Roche, 11836170001). Immunoprecipitations were
180 performed using the indicated primary antibody and Dynabeads™ protein G beads (10004D) at
181 4 °C. The immunoprecipitants were washed at least three times in EBC lysis buffer before being
182 resolved by SDS-PAGE and immunoblotted with indicated antibodies.

183 ***In vivo* modification assays**

184 Cells were solubilized in modified lysis buffer (50 mM Tris, pH 7.4, 150 mM NaCl, 10 % glycerol,
185 1 mM EDTA, 1 mM EGTA, 1 % SDS, 1 mM Na_3VO_4, 1 mM DTT and 10 mM NaF) supplemented
186 with a protease inhibitor cocktail. The cell lysate was incubated at 60 °C for 10 min. The lysate was
187 then diluted 10 times with modified lysis buffer without SDS and incubated with the indicated
188 antibody for 3 h at 4 °C before adding Dynabeads™ protein G beads (10004D). Then the lysate
189 was rotated gently for 8 h at 4 °C. The immunoprecipitants were washed at least three times in wash
190 buffer (50 mM Tris, pH 7.4, 150 mM NaCl, 10 % glycerol, 1 mM EDTA, 1 mM EGTA, 0.1 % SDS,
191 1 mM DTT and 10 mM NaF). Proteins were analyzed by western blotting with indicated antibodies.

192 ***In vitro* modification assays**

193 *In vitro* neddylation was performed using recombinant purified enzymes. GST-PTEN and GST-
194 Ubc12 were expressed in Escherichia coli BL21 (DE3). 0.5 μg of GST-PTEN and 0.5 μg of GST-
195 Ubc12 were incubated with 2 μg of Nedd8, 10 ng of E1 (APPBP1/UBA3) and 0.5 μg of E3 (His-
196 XIAP) in a total reaction volume of 30 μL Nedd8 conjugation Rxn Buffer Kit (Boston Biochem,

197 SK-20). Nedd8 (UL-812), Nedd8 E1 (APPBP1/UBA3) (E-313), His-XIAP were purchased from
198 Boston Biochem. Samples were incubated at 30 ℃ for 1 h, and reactions were terminated with 2 ×
199 SDS-PAGE loading buffer (20 mM Tris-HCl, pH 6.8, 100 mM DTT, 2 % SDS, 20 % glycerol and
200 0.016 % Bromophenol blue) before western blotting. If needed, the neddylation reaction sample
201 was first purified with GST-tag Purification Resin.

202 **Gene reporter assays**

203 MCF-7 cells at 60 %-70 % confluence were transfected using Lipofectamine 3000 (Invitrogen)
204 according to manufacturer's protocol. After 48 hours, cells were lysed in 100 μL of a passive lysis
205 buffer (Promega). Luciferase activity was measured with the Dual Luciferase Assay System
206 (Promega) according to the manufacturer's protocol.

207 **GST pull down**

208 The PTEN or PTEN C2 domain sequence was inserted into the pGEX-4T-3 vector (Amersham). To
209 detect the direct binding, bacteria-expressed GST-tagged proteins were immobilized on
210 BeyoGold™ GST-tag Purification Resin (P2250) and then incubated with Myc-tagged proteins for
211 8 h at 4 ℃ under rotation. Beads were washed with GST-binding buffer (100 mM NaCl, 50 mM
212 NaF, 2 mM EDTA, 1 % NP-40 and protease inhibitor mixture) three times and proteins were eluted,
213 followed by immunoblotting.

214 **Real-time Quantitative RT-PCR**

215 MCF-7 cells were harvested and total RNA was extracted using the TRIzol reagent (Invitrogen)
216 according to the manufacturer's instructions. Reverse transcription of 3 μg total RNA was
217 performed by combining 1 μL ReverTraAce-α-™ (Toyobo. No. FSK-100), 4 μL 5 × buffer, 1 μL
218 10 pmol/μL oligo (dT) primer, 2 μL 10 mM dNTP mix, 1 μL 10 U/μL RNase inhibitor, and water
219 up to a volume of 20 μL. Reaction mixtures were incubated at 30 °C for 10 min, then 42 °C for 20
220 min, 99 °C for 5 min, 4 °C for 5 min and then diluted with 30 μL of water. Each PCR mixture
221 contained 0.5 μL of cDNA template and primers at a concentration of 100 nM in a final volume of

222 25 μL of SYBR green reaction mix (Toyobo. No. QPK-201). Standard curves were calculated using
223 cDNA to determine the linear range and PCR efficiency of each primer pair. Reactions were done
224 in triplicate, and relative amounts of cDNA were normalized to GAPDH. The primers used were
225 listed in Additional file 1: Table S3.

226 **Molecular docking and virtual screening**

227 The molecular docking of PTEN (PDB ID5R) and XIAP (PDB 1C9Q) was performed using the
228 reliable online docking server ZDOCK (http://zdock.umassmed.edu/). The interaction between
229 PTEN and XIAP was visualized using PYMOL version 1.7.0.3. All ten docking complexes were
230 used for our analysis. The cryo-EM structure of human PTEN (PDB ID5R) was used to perform
231 structure-based virtual screening via a workflow application of Glide in Maestro (Schrödinger
232 Maestro 11.4). The Protein-Protein Interaction Library and the MCE Bioactive Compound Library
233 Plus were selected as screening databases. The LigPrep module of Maestro was used to generate
234 the three-dimensional (3D) conformations of the compounds. At the very beginning, the compounds
235 were screened using the high-throughput virtual screening module and the top-ranked 20 %
236 candidates were selected on the basis of the Glide G-score. Then these candidates were redocked
237 using the standard precision and extra precision mode in turn. Finally, 200 compounds with shape
238 rationality and structural diversity were picked for assay.

239 **Surface Plasmon Resonance binding assays (SPR)**

240 Surface plasmon resonance experiments were performed on a BIACORE 3000 biosensor system
241 (GE Healthcare) according to the manufacturer's instructions at 25 °C. PTEN protein was
242 immobilized onto a CM5 chip (GE Healthcare), which was activated using a 1:1 mixture of 1-ethyl-
243 3-(3-dimethyllaminopropyl) carbodiimide (EDC) and N-hydroxysuccinimide (NHS) at a flow rate
244 of 10 μL/min. ECH was diluted in PBS, and then injected over the PTEN surface at a rate of 30
245 μL/min flow rate. The duration of protein binding time was set to 180 s, after which the running
246 buffer was injected at the same rate for 300 s. The binding kinetics were processed and calculated

247 by BIAevaluation software.

248 **Microscale thermophoresis assays (MST)**

249 Microscale thermophoresis assays detected interactions between PTEN and ECH. The
250 concentration of PTEN protein was held constantly at 150 nM, whereas the concentrations of ECH
251 were gradient-diluted (0.0153 μM-500 μM). After brief incubation, the samples were loaded into
252 MST-standard glass capillaries. The measurements were performed on MST machine (NanoTemper
253 Technologies, Munich, Germany).

254 **Thermal shift assay (TSA)**

255 TychoTM NT.6 checked the protein of GST-PTEN quality. Use 10 μL of sample to find out the
256 quality of GST-PTEN protein in 3 minutes and automatically generates thermal unfolding profiles,
257 identifies inflection temperatures (Ti).

258 **Cellular thermal shift assay (CETSA)**

259 HEK293T cells (1×10^7) which transfected Myc-PTEN were resuspended in PBS containing 1 %
260 protease inhibitors. The cells were then lysed by liquid nitrogen through three cycles of freezing
261 and thawing. The resulting cell lysates were centrifuged at 12,000 g for 15 min at 4 °C to collect
262 the supernatants. Subsequently, the samples were divided into 7 equal parts and heated at
263 temperatures of 45 °C, 48 °C, 51 °C, 58 °C, 65 °C, 69 °C, and 72 °C for 3 min each. After heating,
264 the samples were centrifuged at 12, 000 g for 15 min at 4 °C, and the resulting supernatants were
265 collected and boiled with loading buffer. The levels of the target proteins were determined using
266 western blotting.

267 **Cell proliferation assay**

268 Cells were plated on 96-well plates (2000 cells per well). After adding Cell Counting Kit-8 (Dojindo,
269 CK04) to the wells for 1 h, cell numbers were measured at 450 nm. Each cell line was set up in 3
270 replicate wells, and the experiment was repeated three times.

271 **Cell migration assay**

272 Cell migration assay was performed using Cell culture inserts for 24-well plates with 8.0 μm pores
273 filters, and the filter was pre-coated with 20 μg/ml Fibronectin. A cell suspension in serum-free
274 culture medium (5×10^4 cells per well) was added to the inserts, and each insert was placed in the
275 lower chamber containing 10 % FBS culture medium. After 24 h, cells were fixed using 4 %
276 paraformaldehyde for 20 min and stained using 0.1 % crystal violet for 15 min. Cells in upper
277 chamber were carefully removed, and cells migrated through the filter were assessed by
278 photography.

279 **Colony formation assay**

280 Cells were seeded into 6-well tissue culture plate with 2000 cells per well. Plates were incubated at
281 37 °C and 5 % CO_2 and colonies were scored 14 days after preparation. Each cell line was set up
282 in 3 replicate wells, and the experiment was repeated three times.

283 **Fluorescence microscopy**

284 After fixation with 4 % paraformaldehyde and permeabilization in 0.2 % Triton X-100 (PBS), cells
285 were incubated with the indicated antibodies for 12 h at 4 °C, followed by incubation with goat anti
286 rabbit IgG H&L Alexa Fluor 488 or 568 antibody for 1 h at 37 °C. The nuclei were stained with
287 DAPI, and images were visualized with a Leica confocal microscopy.

288 **Tumor organoid culture**

289 The breast cancer tissues were minced and digested with 5 mL of TrypLE (Gibco 12605-010)
290 digestion solution at 37 °C for 1 hour. The digestion was stopped by adding 5 mL of culture medium,
291 followed by centrifugation at 300 g for 5 minutes. The cell pellet was washed with 10 mL of PBS
292 and then filtered through a 70 μm cell strainer. The filtered suspension was centrifuged again at 300
293 g for 5 minutes. Pre-chilled pipette tips were used to resuspend the bottom cells in 50 μL of pre-
294 chilled organoid complete medium and keep them on ice. Then, 250 μL of Matrigel was added to
295 the cell suspension. A pre-warmed 96-well plate was removed, and 30 μL of each drop of the cell
296 suspension was aspirated into the well of the plate using a pre-chilled pipette tip. The plate was

297 quickly inverted and placed in a 37 °C, 5 % CO_2 incubator to allow the matrix gel to solidify for 15
298 minutes. After solidification, an appropriate volume of organoid complete medium was added to
299 each well.

300 **CUT&Tag sequencing**

301 CUT&Tag assay was performed using NovoNGS CUT&Tag 3.0 High-Sensitivity Kit (for Illumina,
302 Novoprotein scientific Inc., Cat#N259-YH01-01A). Briefly, 1×10^5 cells were harvested freshly.
303 Then 37 % formaldehyde was gently added to cells and these samples were incubated at room
304 temperature for 2 min. Cross-linking was stopped by addition of 1.25 M glycine and then the
305 samples were washed with the wash buffer. The cells were enriched by ConA Beads and
306 resuspended by 50 μL primary antibody buffer of anti-JUND antibody, and incubated overnight at
307 4 °C. Then discarded the primary antibody buffer and added 100 μL anti-rabbit IgG antibody buffer
308 for 1 h at a dilution of 1 : 100. Then the beads were washed for 3 times using antibody buffer and
309 then incubated with protein A/G-Tn5 transposome for 1 h and washed for 3 times by ChiTaq buffer.
310 Cells were resuspended in 50 μL Tagmentation buffer and incubated at 37 °C for 1 h. The
311 incubation was stopped by adding 10 μL 10 % SDS at 55 °C for 10 min. The DNA fragments
312 were extracted by Tagment DNA extract beads and amplified using 5 × AmpliMix. Then the DNA
313 was re-extracted by DNA clean beads for sequencing.

314 **Chromatin immunoprecipitation (ChIP) and qChIP**

315 ChIP assays were performed using the EZ-Magna ChIP A/G Chro matin Immunoprecipitation Kit
316 (17-10086, Merck Millipore) according to the manufacturer's recommendations. In brief, the
317 harvested MCF-7 cells were cross-linked with 1 % formaldehyde at 37 °C for 20 min, lysed, and
318 sonicated to generate ~200 to 1000 bp DNA fragments. Antibodies against JUND and rabbit IgG
319 were used for immunoprecipitation, and the precipitated DNA fragments were subjected to qPCR
320 amplification. The primers used were listed in Additional file 1: Table S3.

321 **Flow Cytometry Analysis and FACS Sorting**

322 For detection of apoptosis, cells were co-stained with Annexin-V-phycoerythrin and amino
323 actinomycin D (7-AAD) according to the manufacturer's instructions. Stained cells were sorted
324 with fluorescence-activated cell sorting (FACS). The isolated cell suspension was washed with PBS,
325 then stained with specific mAbs at indicated concentration in PBS solution containing 1 % FBS.
326 Antibody staining was performed at 4 °C for 30 min and the stained cells were analyzed on an
327 LSRFortessa cell analyzer (BD Biosciences). FACS sorting routinely yielded cell purity levels of
328 over 90 %. Data were analyzed using FlowJo software (RRID: SCR_008520).

329 **H&E staining**

330 Haematoxylin-eosin (H&E) staining was performed to examine breast cancer tissue morphology
331 according to standard protocols. In brief, the tissue samples were dehydrated with different
332 concentrations of ethanol and xylol followed by brief washing and staining of cell nuclei with 5 %
333 haematoxylin solution for 10 min. After rinsing in distilled water for 5 min, the stained samples
334 were incubated in 0.1 % HCl-ethanol for 30 s. The samples were then counterstained with eosin
335 solution for 2 min.

336 **Cohort and immunohistochemistry**

337 The breast tissue microarrays were purchased from Shanghai Biochip Company (HBreD090Bc03)
338 and Shanghai Zhuoli Biotech Company (ZL-Brcsur1801). ZL-Brcsur1801 was immunostained
339 with PTEN and Nedd8-PTEN (K402) antibodies (Fig. 1a-c). Detailed pathological information was
340 in Additional file 2: Table S1. HBreD090Bc03 was immunostained with Nedd8-PTEN (K402) and
341 JUND antibodies (Additional file 1: Fig. S2c-f), which are available in Additional file 3: Table S2.
342 In brief, tissues were fixed with 4 % PFA and embedded in paraffin. The samples were then attached
343 to slides, washed and incubated with 3 % H_2O_2 for 10 min. Afterwards, these sections were blocked
344 and then incubated with a primary antibody at 4 °C overnight. After washing with PBS, the sections
345 were incubated with secondary antibody for 1 h at room temperature. Finally, the sections were
346 washed and incubated with DAB substrate for visualization. After washing and dehydration, the

347 sections were sealed with coverslips. All staining was assessed by a quantitative imaging method;
348 the percentage of immunostaining and the staining intensity were recorded. An H-score was
349 calculated using the following formula: H-score = Σ (PI × I) = (percentage of cells of weak
350 intensity × 1) + (percentage of cells of moderate intensity × 2) + (percentage of cells of strong
351 intensity × 3). PI indicates the percentage of positive cells versus all cells.

352 **Multiplex immunohistochemical**

353 Pheno 7-plex IHC kit (Pheno, PVB2002) was used according to manufacturer's protocol. Slides
354 were deparaffinised in xylene and rehydrated with ethanol and double distilled water. Antigen was
355 retrieved by citrate buffer and heated to boil in microwave for approximately 20 min, sections were
356 then blocked with bovine serum albumin at room temperature for 10 min. Primary antibodies were
357 incubated at 37 °C for 30 min, secondary antibody conjugated with horseradish peroxidase was
358 incubated at room temperature for 10 min. Tyramide signal amplification was performed with 1 :
359 100 in antibody dilution buffer diluted fluorophores and incubated at room temperature for 10 min.
360 Nuclei were stained with DAPI after primary antibodies were stained.

361 **ELISA assay**

362 The quantitation of IL-1β, IL-17A and G-CSF levels in MCF-7 cells were performed using ELISA
363 assay kit (Solarbio, SEKM-0002, SEKH-0026, and SEKH-0058) according to the manufacturer's
364 instructions.

365 **Immunoassay arrays**

366 Cytokine concentrations of supernatants of indicated cells were measured using the CBA
367 (Cytometric Bead Array, RayBiotech FAH-STRM-1) following the manufacturer' s instruction.
368 Read samples on a flow cytometer and analyze using FCAP Array software (BD Biosciences).

369 **Statistical analysis**

370 All data were representative of no fewer than three independent experiments. All data were
371 presented as means ± S.D. Data were analyzed using SPSS 19.0 (IBM Corp., Armonk, NY, USA,

372 RRID: SCR_002865) and GraphPad Prism 8 (GraphPad Software, Inc., La Jolla, CA, RRID:
373 SCR_002798). The differences between groups were assessed by Student's *t*-test or one-way
374 ANOVA test. The correlations were analyzed using the pearson correlation test. A value of $P < 0.05$
375 was considered to be statistically significant.

376 **Results**

377 **Resistance to CDK4/6 inhibitor upregulates PTEN neddylation in breast cancer**

378 We previously found that elevated PTEN neddylation in breast cancer correlates with poor clinical
379 outcomes [30], and we confirmed those results here (Fig. 1a, b). We observed that PTEN
380 neddylation was upregulated in all breast cancer subtypes, particularly in luminal-type cancers,
381 while PTEN was downregulated in all subtypes without distinction (Fig. 1c). Detailed pathological
382 information was showed in Additional file 2: Table S1. Palbociclib, one kind of CDK4/6 inhibitor,
383 has been widely used for the treatment of advanced breast cancer patients. Using the antibody that
384 specifically recognized PTEN neddylation, our results showed that PTEN neddylation was
385 markedly upregulated in palbociclib-resistant breast cancer patients with recurrence *in situ* and liver
386 metastasis, while PTEN remained lowly expressed in drug-resistant patients (Fig. 1d). Pathological
387 data of the patients were provied (Additional file 1: Fig. S1a). Next, we monitored MMTV-*PyMT*
388 (C57BL/6J background) transgenic mice, which spontaneously develop luminal breast tumors, as
389 a model for late-stage luminal breast cancer [32-34]. Through daily palbociclib treatment, by day
390 20, tumor volumes and sizes in treated mice showed no difference from those in the control group,
391 indicating the onset of drug resistance (Fig. 1e-h). Rb is a tumor suppressor that is phosphorylated
392 during the transition from G1 to S phase of the cell cycle by CDK4/6. When CDK4/6 inhibitors are
393 ineffective, phosphorylation of the Rb protein would become uncontrolled [35]. Therefore, the
394 increased phosphorylation of the Rb protein in the mice also indicated the occurrence of drug
395 resistance (Fig. 1i, j). More importantly, high levels of PTEN neddylation were detected in
396 palbociclib-resistant breast tumor tissues of MMTV-*PyMT* mice, while the expression of PTEN

397 remained unchanged (Fig. 1i, j). Additionally, we found that the IC50 of breast tumor cells isolated
398 from palbociclib-resistant MMTV-*PyMT* mice was significantly higher compared to the
399 palbociclib-sensitive group (Fig. 1k), indicating the development of drug resistance. Taken together,
400 our data revealed that PTEN neddylation exhibited elevated levels in palbociclib-resistant breast
401 cancer.

402 **Increased XIAP leads to enhanced PTEN neddylation in palbociclib-resistant breast cancer**

403 To explore the underlying mechanisms of elevated PTEN neddylation in palbociclib-resistant breast
404 cancer, we generated acquired palbociclib-resistant breast cancer stable cell lines (MCF-7-PR).
405 Dose-response curves results showed that palbociclib-resistant cells were more resistant to
406 palbociclib than the parental cells (Fig. 2a). Compared with the parental cells, the palbociclib-
407 resistant cells exhibited accelerated G1/S phase and cell proliferation ability after treatment of
408 palbociclib (Fig. 2b, c). Consistently, PTEN neddylation was upregulated in acquired palbociclib-
409 resistant breast cancer cells (Fig. 2d). Moreover, the ubiquitination of PTEN was unchanged in
410 palbociclib-resistant cells (Additional file 1: Fig. S1b). Compared to other drug-resistant breast
411 cancer cell lines, such as MCF-7 sublines resistant to doxorubicin (MCF-7/ADR), cisplatin (MCF-
412 7/DDP), and paclitaxel (MCF-7/PTX), PTEN neddylation was specifically increased in palbociclib-
413 resistant breast cancer cells (Fig. 2e). Short-term drug treatment could induce adaptive resistance
414 in cells [13]. We noticed that the phosphorylation of Rb, initially reduced by palbociclib treatment,
415 recovered after prolonged drug exposure, which indicated adaptive resistance was occurred (Fig.
416 2f). Under the adaptive resistance, PTEN neddylation was increased and could be reduced by
417 MLN4924, which was the inhibitor of neddylation E1 (Fig. 2f, g left pannels). For ER negative
418 cells, such as glioma cells T98G, show reduced palbociclib sensitivity [36]. As expected, no
419 obvious changes in PTEN neddylation or p-Rb were detected when the T98G cells were treated
420 with palbociclib (Fig. 2g right panels).

421 Then, we intended to explore the mechanism of high PTEN neddylation in palbociclib-resistant
422 breast cancer. Notably, our data revealed that XIAP, the E3 ligase for PTEN neddylation [30], was
423 upregulated in palbociclib-resistant breast cancer cells, while no significant changes were observed
424 in Nedd8 E1-UBA3, Nedd8 E2-Ubc12, and Nedd8 (Fig. 2h). The increased XIAP enhanced the
425 interaction with PTEN in both early adaptative palbociclib-resistant and acquired palbociclib-
426 resistant breast cancer cells (Fig. 2i-k). The above data suggested that high PTEN neddylation in
427 palbociclib-resistant breast cancer cells was likely due to XIAP upregulation and increased XIAP-
428 PTEN interaction.

429 **PTEN neddylation enhances the protein stability of JUND**

430 In previous studies, we have demonstrated that Nedd8 is covalently attached to lysine residues at
431 positions 197 and 402 of PTEN [30]. To examine the role of PTEN neddylation on CDK4/6i
432 resistance, we performed RNA-seq in palbociclib-resistant breast cancer cells (Fig. 3a) and PTEN
433 neddylation deficient cells (2KR, K197 and K402 sites mutated to R) (Fig. 3b). Other than the
434 PI3K/Akt signaling pathway, which has been believed to be highly associated with CDK4/6i
435 resistance and PTEN neddylation, we noticed that MAPK, as well as JAK/STAT signaling
436 pathways were also enriched (Fig. 3a, b). GSEA analysis further indicated that MAPK signaling
437 pathway obviously was also enriched in both palbociclib-resistant breast cancer cells (Fig. 3c) and
438 PTEN neddylation deficient cells (Fig. 3d). Similar data were shown in the related dataset
439 (GSE222367) (Additional file 1: Fig. S2a). AP-1 (Activator Protein-1) transcription factors are
440 heterodimers or homodimers composed of JUN and FOS proteins. AP-1 is known to be activated
441 by MAPK signaling pathways through the phosphorylation of JUN and FOS proteins, and in turn,
442 AP-1 also regulates the expression of genes involved in MAPK signaling pathways [37]. The
443 reporter gene assays revealed that AP-1 transcription factor activity was significantly increased
444 after palbociclib resistance developed (Fig. 3e). Further heat map data showed that palbociclib
445 resistance led to the upregulation of AP-1 related transcription factors, including *FOSB*, *FOSL*, *c-*

446 *FOS*, *c-JUN*, *JUND*, and *JUNB* (Fig. 3f and Additional file 1: Fig. S2b). Conversely, PTEN
447 neddylation deficiency decreased the expression of those genes (Fig. 3g). Then, we detected the
448 protein levels of the AP-1 transcriptional factors and noticed that there was a markable increase of
449 JUND in palbociclib-resistant cells (Fig. 3h). Meanwhile, the activated form of JUND,
450 phosphorylated JUND, was also upregulated when cells were resistant to palbociclib (Fig. 3i).
451 Similar results were also found in early adaptive palbociclib-resistant MCF-7 cells and palbociclib-
452 resistant breast cancer tissues in MMTV-*PyMT* mice, but not in ER-negative T98G cells (Fig. 3j,
453 k). Next, analysis of nuclear and cytoplasmic fractions revealed that, in palbociclib-resistant breast
454 cancer cells, JUND and phosphorylated JUND were significantly elevated, primarily in the nucleus
455 (Fig. 3l). Finally, the results showed that JUND was also markedly upregulated in palbociclib-
456 resistant breast cancer patients (Fig. 3m). These results strongly suggest that the MAPK/AP-1
457 signaling pathway is a key mechanism of resistance to palbociclib, and PTEN neddylation
458 upregulates JUND protein expression while regulating AP-1 activity.

459 **PTEN neddylation decreases JUND ubiquitination**

460 Next, we intended to explore the mechanism by which PTEN neddylation promotes JUND protein
461 expression, IP analysis indicated that the ubiquitination of JUND was obviously decreased in
462 palbociclib-resistant breast cancer cells (Fig. 4a). We generated a fusion protein (PTEN-Nedd8) by
463 linking Nedd8 to the C-terminus of PTEN to mimic neddylated PTEN. Neddylation would promote
464 PTEN nuclear translocation. Therefore, a nuclear localization sequence (NLS) was fused to the N-
465 terminus of PTEN to generate NLS-PTEN for comparison [30, 38, 39]. Then we observed an
466 increased expression level of JUND and phosphorylated JUND in sh*PTEN*+PTEN-Nedd8 MCF-7
467 cells, but the opposite effect was found in sh*PTEN*+PTEN-NLS MCF-7 cells (Fig. 4b). Compared
468 with NLS-PTEN, JUND showed a higher affinity for neddylated PTEN (Fig. 4c). Moreover,
469 enhanced interaction between neddylated PTEN and JUND reduced JUND ubiquitination (Fig. 4d).
470 Next, we confirmed that JUND expression was significantly increased in tumor tissues compared

471 with matched adjacent normal tissues, particularly in luminal-type breast cancer (Additional file 1:
472 Fig. S2c, d). By comparison, the levels of JUND and neddylated PTEN were positively correlated
473 in luminal-type breast cancer (Additional file 1: Fig. S2e, f). Detailed pathological information was
474 in Additional file 3: Table S2.

475 To date, no specific ubiquitin ligase for JUND has been reported. Through UbiBrowser 2.0 [40, 41],
476 ITCH (also known as AIP4) was predicted to be the E3 of JUND with the highest affinity among
477 the interactive protein candidates (Additional file 1: Fig. S2g). As expected, overexpression of
478 ITCH reduced the levels of JUND protein and its phosphorylation, however, this negative
479 regulatory effect was significantly diminished after palbociclib resistance developed (Fig. 4e).
480 Overexpression of ITCH promoted ubiquitination of JUND (Fig. 4f). Considering that neddylated
481 PTEN in the nuclear intended to regulate the protein-protein interactions, we first used molecular
482 docking with AlphaFold 2.0 to evaluate whether neddylation of PTEN affects the interaction
483 between ITCH and JUND. The results indicated that neddylated PTEN could occupy the binding
484 region between ITCH and JUND, whereas PTEN without Nedd8 could not (Fig. 4g). We then
485 evaluated the interaction between ITCH and JUND and found that JUND was unable to bind to
486 ITCH in sh*PTEN*+PTEN-Nedd8 MCF-7 cells (Fig. 4h, i). Furthermore, JUND failed to interact
487 with ITCH in the palbociclib-resistant breast cancer cells compared to the palbociclib-sensitive cells
488 (Fig. 4j). Collectively, the results indicate that during drug resistance, elevated PTEN neddylation
489 interferes with the interaction between JUND and its ubiquitin ligase, reducing JUND
490 ubiquitination and increasing its protein stability.

491 **Identification of Echinacoside as a PTEN neddylation inhibitor**

492 The above data indicate that PTEN neddylation is a key factor contributing to resistance against
493 palbociclib treatment. Next, we aimed to explore the possibility of disrupting the interaction
494 between PTEN and XIAP to reduce PTEN neddylation in tumor cells, and thus overcoming
495 resistance to palbociclib. Consistent with previous study [30, 42], XIAP was co-

496 immunoprecipitated with PTEN *in vivo* (Additional file 1: Fig. S3a). The truncations containing the
497 BIR2 domain of XIAP and the C2 domain of PTEN interacted with each other (Fig. 5a and
498 Additional file 1: Fig. S3b-d). Then, molecular docking and *in vitro* pull-down assay indicated that
499 Y154 and N234 sites at XIAP, as well as S207 and R335 sites at PTEN were key binding sites on
500 the interaction surface (Fig. 5b, c). On the basis of the binding determinants of the XIAP-PTEN
501 interface, structure-based virtual screening was performed to find potential XIAP-PTEN PPI
502 (protein and protein interaction) inhibitors (Fig. 5d). Ultimately, we selected top five compounds,
503 guided by the top-ranking binding models and docking scores from the Enamine libraries
504 containing protein-protein interacting compounds and the Bioactive Compound Library Plus at *Med*
505 *Chem Express* LLC (Additional file 1: Fig. S3e). No PPI inhibitors affected the protein and mRNA
506 levels of PTEN (Additional file 1: Fig. S3f, g). All the five compounds inhibited PTEN neddylation,
507 with Echinacoside (ECH) and Z219118374 showing the most significant inhibition effect
508 (Additional file 1: Fig. S3h). We noticed that Echinacoside (ECH), a natural phenylethanoid
509 glycoside, had the highest molecular docking score and formed hydrogen bonds with the critical
510 PTEN residues S207 and R335 that interacted with XIAP (Fig. 5e, f). ECH is one of the main
511 phenylethanol glycosides isolated and purified from *cistanche tubulosa*, which has been used as
512 traditional Chinese herbal medicine with anti-senility and antifatigue effects [43, 44]. Subsequently,
513 we employed surface plasmon resonance and microscale thermophoresis assay to evaluate the
514 interaction between ECH and PTEN. As illustrated in Fig. 5g and 5h, ECH showed a high-affinity
515 binding with PTEN. In addition, TSA assay showed that the inflection temperature (Ti) of GST-
516 PTEN increased after co-incubation with ECH (Additional file 1: Fig. S3i). Next, we monitored
517 ECH binding with PTEN using the cellular thermal shift assay. The obvious shift in the melting
518 curve indicated increased PTEN protein stability and high-affinity binding upon addition of ECH
519 (Fig. 5i). Furthermore, ECH effectively disrupted the interaction between XIAP and PTEN *in vivo*
520 (Fig. 5j). The pull-down assay revealed a clear dose-dependent decrease in the interaction between

521 XIAP and the PTEN C2 domain following ECH treatment. (Fig. 5k). Moreover, ECH did not affect
522 the dimerization of PTEN (Additional file 1: Fig. S3j, k).

523 To determine whether ECH could disrupt PTEN neddylation, we performed *in vivo* and *in vitro*
524 neddylation assays. The results revealed that ECH reduced PTEN neddylation, but not
525 ubiquitination (Fig. 5l). *In vitro* neddylation assay indicated that ECH directly interfered XIAP
526 mediated PTEN neddylation (Fig. 5m). As expected, elevated JUND levels, JUND phosphorylation,
527 and Akt phosphorylation, which increased after palbociclib resistance, were diminished following
528 ECH treatment (Fig. 5n). Additionally, there was a significant increase in JUND ubiquitination and
529 decrease in AP-1 transcriptional activity following ECH treatment (Fig. 5o, p). Taken together, we
530 identified Echinacoside as a potent PTEN neddylation inhibitor that eliminates PTEN neddylation
531 by inhibiting the interaction between XIAP and PTEN.

532 **ECH depends on PTEN neddylation to suppress tumorigenesis**

533 Then, we intended to explore the role of ECH in tumorigenesis. ECH exhibited a significant tumor-
534 suppressive effect, manifested in a dose-dependent manner, on cellular proliferation, colony
535 formation, and cell migration across various tumor cell lines (Additional file 1: Fig. S4a-d). We
536 measured drug toxicity of ECH in CD-1 mice and found no significant differences in body weight
537 (Additional file 1: Fig. S5a, b), blood cell counts or composition (Additional file 1: Fig. S5c), or
538 serum ALT levels (Additional file 1: Fig. S5d), indicating no obvious liver injury. Additionally,
539 ECH treatment showed no signs of toxicity or organ damage based on weight and histopathology
540 of vital organs (Additional file 1: Fig. S5e-g). Thus, we speculated that ECH might have substantial
541 anti-tumor efficacy with minimal adverse effects.

542 To be note, deletion of *PTEN* significantly weakened the inhibitory effects of ECH on cell
543 proliferation (Fig. 6a, b) and tumor invasion (Fig. 6c). Moreover, palbociclib inhibited cell
544 proliferation (Fig. 6d, e) and increased the cell death (Fig. 6f) in PTEN neddylation deficient cells.
545 However, ECH was unable to inhibit tumor cell proliferation when PTEN neddylation was deficient

546 (Fig. 6g, h). Additionally, in PTEN neddylation-deficient cells, ECH no longer reduced the protein
547 levels of JUND and p-JUND (Fig. 6i), nor did it decrease AP-1 activity (Fig. 6j). Furthermore,
548 CUT&Tag analysis performed on PTEN neddylation-deficient cells indicated an enrichment of the
549 PI3K/Akt signaling pathway and the MAPK/AP-1 signaling pathway (Fig. 6k, l). The data
550 demonstrated that in the absence of PTEN neddylation, JUND exhibited reduced enrichment at the
551 promoters of downstream genes associated with inflammation and immune responses, including
552 CSF2, IL-17, IL-6, MMP13, and IL-1β (Fig. 6m). Due to the significant changes in these genes, an
553 immunoassay array was performed. As shown in Fig. 6n and 6o, the results demonstrated a
554 reduction in multiple cytokines and chemokines, including G-CSF, GM-CSF, IFN-γ, IL-1RA, IL-
555 1β, IL-8, CCL2/4, IL-17, and VEGF, following ECH treatment. However, no alterations were
556 observed in the PTEN neddylation deficient cells subsequent to ECH exposure. Similar results of
557 G-CSF, IL-1β, IL-17 were also approved by ELISA assay (Fig. 6p). Therefore, the above evidence
558 suggested that ECH inhibited oncogenic effects, at least to some extent, by interfering with PTEN
559 neddylation.

560 **Combination ECH enhances the sensitivity of palbociclib in breast cancer**

561 We next aimed to explore whether ECH could overcome palbociclib resistance in breast cancer. As
562 expected, the tumor weight and volume were both markedly declined in the palbociclib resistance
563 MMTV-*PyMT* mice following the treatment of ECH (Fig. 7a-d). Similar results were also obtained
564 from the primary breast cancer cells isolated from MMTV-*PyMT* mice (Additional file 1: Fig. S6a,
565 b), and the tumor organoids established from them (Additional file 1: Fig. S6c-e). In immunoassay
566 arrays, there was an obvious reduction of GM-CSF and G-CSF following ECH treatment (Fig. 6n,
567 o). G-CSF is well known to function as a mobilizing agent for neutrophils, while GM-CSF
568 influences the development and functionality of both neutrophils and macrophages [45-47].
569 Immunohistochemistry and flow cytometry showed a significant reduction in the population of
570 active neutrophils labeled by $Ly6G^{+}$, $CD11b^{+}$, and $CD62L^{-}$ in palbociclib-resistant MMTV-*PyMT*

571 mice after ECH treatment (Fig. 7e, f). We confirmed a decrease in JUND, phosphorylation of Akt,
572 PTEN neddylation, and XIAP levels, with no notable changes in neddylation of E1-UBA3, E2-
573 Ubc12, and Nedd8 in palbociclib-resistant breast cancer tissues from MMTV-*PyMT* mice after
574 ECH treatment (Additional file 1: Fig. S6f-i). The combination of ECH with palbociclib showed
575 significantly decreased cell proliferation compared with monotherapy (Fig. 7g). In the ER-negative
576 T98G cells, which was resistance to palbociclib, the co-administration of ECH increased sensitivity
577 to palbociclib, thereby suppressing tumor cell proliferation (Additional file 1: Fig. S7a, b). We
578 finally intended to confirm the efficacy of combination therapy using tumor organoid models
579 derived from the human luminal breast cancer patient. Both ECH and palbociclib monotherapies
580 demonstrated tumor growth suppression effects, but the combination treatment exhibited even
581 better anti-tumor growth efficacy compared with the monotherapies (Fig. 7h, i).
582 Immunofluorescence staining showed a significant reduction in PTEN neddylation following ECH
583 treatment in the E-cadherin positive organoids (Fig. 7j). Taken together, these findings collectively
584 illustrate that ECH serves as an effective sensitizing agent for palbociclib in breast cancer, with the
585 combined therapy showing a better anti-tumor activity.

586 **Discussion**

587 For luminal breast cancer patients, the standard treatment consists of CDK4/6 inhibitors combined
588 with endocrine therapy. However, since resistance to CDK4/6 inhibitors is inevitable, there is
589 considerable focus on developing therapeutic strategies to overcome this resistance. Here, we
590 demonstrate that a post-translational modification of PTEN, namely neddylation, contributes to
591 CDK4/6 inhibitor resistance in breast cancer. We firstly prepared antibodies that specifically
592 recognize PTEN neddylation modification. Then, increased PTEN neddylation was observed in
593 breast cancer patients resistant to palbociclib, as well as in both palbociclib-resistant breast cancer
594 cells and spontaneous breast cancer MMTV-*PyMT* mice. Our previous data defined neddylation as
595 a critical modification of PTEN, which inhibits PTEN tumor suppressor function and activates the

596 PI3K/Akt signaling pathway, revealing a previously unidentified tumor-promoting role of
597 neddylated PTEN [30]. Palbociclib resistance upregulated PTEN neddylation *via* the E3 ligase
598 XIAP, consistent with previous studies suggesting that compensatory CDK2 activation upon
599 resistance increases XIAP mRNA levels [48, 49]. This dynamic resulted in enhanced binding to
600 PTEN, thereby contributing to the augmented PTEN neddylation and hyperactivated PI3K/Akt
601 signaling pathway observed following palbociclib resistance.
602 *PIK3CA* mutations occur in approximately 40 % of luminal breast cancers, and activation of the
603 PI3K/Akt signaling pathway is prominent as cancers become resistant to CDK4/6 inhibitors [15].
604 While PI3K inhibitors hold promise in mitigating the onset of CDK4/6 inhibitor resistance, their
605 efficacy in rescuing cells from established resistance falls short, as they are unable to reverse the
606 acquired insensitivity [50-52]. Apart from the upregulation of PI3K/Akt signaling pathway, our
607 study showed that the increase in PTEN neddylation after palbociclib resistance led to the over-
608 activation of the MAPK/AP-1 signaling pathway. Mechanistically, we identified that neddylated
609 PTEN interacted with JUND. JUND is a component protein of the activating protein-1 (AP-1)
610 transcription factor and is considered as a classical proto-oncogene. Dysfunctional AP-
611 1 transcriptional activity is associated with tumor growth, invasion, migration and drug resistance
612 [37, 53, 54]. So far, it is known that CDK4/6 inhibition reprograms the breast cancer enhancer
613 landscape by stimulating AP-1 transcriptional activity [55]. However, the role of AP-1 in regulating
614 resistance to CDK4/6 inhibitors remains unclear. Here, we reported that PTEN neddylation led to
615 an obviously enhancement in JUND protein stability in palbociclib resistance breast cancer cells
616 and mouse models. The expression of JUND in palbociclib-resistant patients showed a positive
617 correlation with the PTEN neddylation modification level and a negative correlation with PTEN
618 expression. Up to day, no ubiquitin ligase has been clearly reported to catalyze the ubiquitination
619 mediated degradation of JUND. We identified that ITCH as a polyubiquitination E3 ligase for
620 JUND. However, under the palbociclib-resistant conditions, ITCH no longer promoted JUND

621 ubiquitination and reduced its protein stability. Further structural docking and immunoprecipitation
622 assays showed that neddylated PTEN interfered with the interaction between JUND and ITCH,
623 reducing the ubiquitination of JUND catalyzed by ITCH, thereby preventing the degradation of
624 JUND. Therefore, the increased modification of PTEN neddylation after palbociclib resistance
625 enhanced the protein stability and phosphorylation level of JUND, thereby activating the AP-1
626 transcription factor activity. Thus, further data showed that the expression levels of JUND
627 downstream target genes such as CSF2, IL-1β, IL-6, IL-17, and MMP13 were increased. These
628 results propose a novel role for PTEN neddylation in upregulating AP-1 transcription factor activity
629 and activating the MAPK/AP-1 signaling pathway during resistance to palbociclib treatment.
630 Neddylation is indispensable in various cellular processes and homeostasis, but excessive activation
631 of this modification has been observed in numerous tumors. Small molecules targeting neddylation
632 activating enzymes (E1), such as MLN4924 (trade name pevonedistat) and TAS4464, have shown
633 promise in clinical trials for cancer treatment [28, 56]. DI-404, DI-591, NAcM-HIT, NAcM-OPT,
634 and WS-383 are competitive neddylation conjugating enzymes (E2) inhibitors that target UBE2M-
635 DCN1 interaction [57-59]. HA-9104 is a targeted inhibitor of another E2-UBE2F [60]. Given the
636 limited number of neddylation E1 and E2 enzymes, inhibiting neddylation broadly may pose
637 inevitable cytotoxicity and drug safety concerns. Therefore, for tumor treatment, more specific and
638 targeted drugs are needed to address neddylation modifications. No small molecule drugs
639 specifically targeting neddylation substrates have been reported, but we believe that would offer
640 greater specificity, reduced drug side effects, and potentially more potent anti-tumor effects. XIAP
641 has been identified as a specific ligase for PTEN neddylation both *in vivo* and *in vitro* [30]. Next,
642 we employed a specific small molecule inhibitor, Echinacoside (ECH), to interfere with the
643 dynamic interplay between XIAP and PTEN, ultimately suppressing the neddylation of PTEN both
644 *in vivo* and *in vitro*. ECH, a key efficacious constituent found in *Echinacea*, is also abundantly
645 present in various other natural plant sources, including the roots of *Scrophulariae*, *Rehmanniae*,

646 and *Cistanches Herba*, among others [43, 44]. It has been reported that ECH inhibits tumor
647 metastasis *via* suppressing the PI3K/AKT signaling pathway, but the mechanism remains unclear
648 [61-63]. Our research demonstrates that ECH exhibits excellent anti-tumor efficacy through its
649 effect on PTEN neddylation. For the first time, our study demonstrates that ECH is a selective
650 inhibitor targeting neddylation substrates.

651 Although the resistance mechanisms associated with CDK4/6 inhibitors in breast cancer have been
652 documented, but not fully elucidated. For instance, the concurrent use of PI3K inhibitors like
653 alpelisib or buparlisib with CDK4/6 inhibitors is discouraged due to safety concerns [14, 15]. Since
654 PTEN is a key suppressor in the PI3K/Akt pathway, restoring its tumor-suppressive function could
655 more effectively inhibit this pathway [23]. More importantly, our data reported that ECH obviously
656 elevates the sensitivity of palbociclib, and ECH in combination with palbociclib would more
657 effectively reduce the tumor growth. In the tumor microenvironment, the role of neutrophils is
658 complex and multifaceted, highly correlated with the development of drug resistance [64, 65]. Our
659 data showed that the number of activated neutrophils increases after palbociclib resistance,
660 accompanied by an increase in various pro-inflammatory factors and growth factors, such as G-
661 CSF, GM-CSF, IL-1β, VEGF. Treatment with ECH was observed to decrease activated neutrophils
662 following palbociclib resistance. Future study needs to explore the role of activated neutrophils in
663 ROS production and the immunosuppressive microenvironment, and discuss the function of other
664 different terms of neutrophils. Ultimately, our findings unlock a promising therapeutic strategy by
665 focusing on neddylation to effectively restore PTEN tumor suppressor activity, thereby enhancing
666 the efficacy of palbociclib (Fig. 7k). It highlights a deeper understanding of CDK4/6i resistance
667 mechanisms and the development of advanced combination therapies in optimizing breast cancer
668 treatment outcomes.

669 **Conclusions**

670 In conclusion, we demonstrate, for the first time, that the neddylation modification of PTEN is
671 significantly elevated in breast cancer patients resistant to CDK4/6 inhibitors. Mechanistically,
672 neddylated PTEN enhances AP-1 transcriptional activity by stabilizing the JUND protein.
673 Ultimately, Echinacoside interrupts PTEN neddylation to overcome CDK4/6 inhibitor resistance.
674 We propose targeted intervention to inhibit PTEN neddylation as a novel strategy to effectively
675 restore tumor suppressor activity, marking a groundbreaking approach in overcoming resistance
676 and cancer therapy.

677 **Abbreviations**

678 CDK4/6i: cyclin D-dependent kinases 4 and 6 inhibitor; PTEN: phosphatase and tension
679 homologue deleted from chromosome 10; ECH: echinacoside; MCF-7-PS: palbociclib-sensitive
680 breast cancer cell lines; MCF-7-PR: acquired palbociclib-resistant breast cancer stable cell lines;
681 MCF-7/ADR: MCF-7 sublines resistant to doxorubicin; MCF-7/DDP: MCF-7 sublines resistant to
682 cisplatin; MCF-7/PTX: MCF-7 sublines resistant to paclitaxel; PDOs: patient-derived organoids;
683 HR+: hormone receptor-positive; HER2-: human epidermal growth factor receptor 2-negative; Rb:
684 retinoblastoma; FDA: the US food and drug administration; 2KR: K197 and K402 sites mutated to
685 R; NLS: nuclear localization sequence; AP-1: activator protein-1; PPI: protein and protein
686 interaction; DMSO: dimethyl sulfoxide; 3D: three-dimensional; TME: tumor microenvironment;
687 H&E: hematoxylin & eosin; EBC: elution buffer for cell lysis; SDS-PAGE: sodium dodecyl sulfate-
688 polyacrylamide gel electrophoresis; SD: standard deviation; RNA-seq: RNA-sequencing; FPKM:
689 Fragments Per Kilobase of exon model per Million mapped fragments GSEA: gene set enrichment
690 analysis; ELISA: enzyme-linked immunosorbent assay; KEGG: kyoto encyclopedia of genes and
691 genomes; ChIP: chromatin immunoprecipitation; IHC: immunohistochemistry; SPR: surface
692 plasmon resonance binding assays; MST: microscale thermophoresis assays; TSA: thermal shift
693 assay; CETSA: cellular thermal shift assay.

694 **Supplementary Information**

695 **Additional file 1:**

696 Figure S1. PTEN neddylation modification is upregulated in the CDK4/6 inhibitor-resistant breast
697 cancer.

698 Figure S2. PTEN neddylation enhances JUND stability in palbociclib-resistant breast cancer.

699 Figure S3. Echinacoside inhibits the binding of PTEN and XIAP to suppress PTEN neddylation.

700 Figure S4. ECH inhibits the tumor cell invasion and proliferation.

701 Figure S5. ECH exhibits low toxicity in CD-1 non-tumor-bearing mice.

702 Figure S6. ECH resists CDK4/6 inhibitor resistance in MMTV-*PyMT* breast cancer mice.

703 Figure S7. Combination of ECH enhances the sensitivity of palbociclib in breast cancer.

704 Table S3: Primers.

705 **Additional file 2:** Table S1, List of pathological information of ZL-Brcsur1801.

706 **Additional file 3:** Table S2, List of pathological information of HBreD090Bc03.

707 **Declarations**

708 **Ethics approval and consent to participate**

709 All animals were handled in strict accordance to the "Guide for the Care and Use of Laboratory
710 Animals" and the "Principles for the Utilization and Care of Vertebrate Animals", and all animal
711 work was approved by Capital Medical University Ethics Committee. The clinical samples were
712 approved by the department of breast and thyroid surgery at the Second People's Hospital of
713 Shenzhen and Hunan Cancer Hospital. Informed consent was obtained from all subjects or their
714 relatives.

715 **Consent for publication**

716 All authors have agreed to publish this manuscript.

717 **Acknowledgements**

718 Thanks to Core Facility Center, Capital Medical University for providing platform support for
719 this research.

720 **Competing interests**

721 The authors declare that there are no competing financial, commercial, or professional interest that
722 could influence the performance, interpretation, or reporting of the research presented in this
723 manuscript. All authors have read and approved this declaration of interests, confirming that it
724 accurately reflects their current situation.

725 **Data and materials availability**

726 RNA-seq data have been deposited at SRA (PRJNA1143082 and PRJNA1144658) and are publicly
727 available as of the date of publication. All data are available in the main text or the supplementary
728 materials.

729 **Funding**

730 National Outstanding Youth Science Fund Project of National Natural Science Foundation of
731 China grant 82122052 (PX)

732 The National Natural Science Foundation of China (NSFC) grant No. 32471305 (PX)

733 Outstanding Young Talents Program in Chinese Institutes for Medical Research, Beijing grant
734 CX23YQA03 (PX)

735 **Author's contributions**

736 Conceptualization: PX; Methodology: FL, WXL, YXS, SHL, XKJ; Formal Analysis: FL;
737 Investigation: PX, FL; Resources: SYS, YWT, ZZ; Writing-Original Draft: PX; Funding
738 Acquisition: PX

739 **References**

740 1. Nolan E, Lindeman GJ, Visvader JE. Deciphering breast cancer: from biology to the clinic. Cell.
741 2023;186:1708–1728.

742 2. Harbeck N, Gnant M. Breast cancer. Lancet. 2017;389:1134–1150.

743 3. Giuliano M, Schettini F, Rognoni C, Milani M, Jerusalem G, Bachelot T, et al. Endocrine
744 treatment versus chemotherapy in postmenopausal women with hormone receptor-positive, HER2-
745 negative, metastatic breast cancer: a systematic review and network meta-analysis. Lancet Oncol.
746 2019;20:1360-1369.

747 4. Goel S, Bergholz JS, Zhao JJ. Targeting CDK4 and CDK6 in cancer. Nat Rev Cancer.
748 2022;22:356–372.

749 5. Morrison L, Loibl S, Turner NC. The CDK4/6 inhibitor revolution - a game-changing era for
750 breast cancer treatment. Nat Rev Clin Oncol. 2024;21:89–105.

751 6. O'Sullivan CC, Clarke R, Goetz MP, Robertson J. Cyclin-Dependent Kinase 4/6 Inhibitors for
752 Treatment of Hormone Receptor-Positive, ERBB2-Negative Breast Cancer: A Review. JAMA
753 Oncol. 2023;9:1273–1282.

754 7. Portman N, Alexandrou S, Carson E, Wang S, Lim E, Caldon CE. Overcoming CDK4/6 inhibitor
755 resistance in ER-positive breast cancer. Endocr Relat Cancer. 2019;26:R15–R30.

756 8. Lloyd MR, Spring LM, Bardia A, Wander SA, Mechanisms of Resistance to CDK4/6 Blockade
757 in Advanced Hormone Receptor-positive, HER2-negative Breast Cancer and Emerging
758 Therapeutic Opportunities. Clin Cancer Res. 2022;28:821–830.

759 9. Cai Z, Wang J, Li Y, Shi Q, Jin L, Li S, et al. Overexpressed Cyclin D1 and CDK4 proteins are
760 responsible for the resistance to CDK4/6 inhibitor in breast cancer that can be reversed by
761 PI3K/mTOR inhibitors. Sci China Life Sci. 2023;66:94–109.

762 10. Palafox M, Monserrat L, Bellet M, Villacampa G, Gonzalez-Perez A, Oliveira M, et al. High
763 p16 expression and heterozygous RB1 loss are biomarkers for CDK4/6 inhibitor resistance in ER(+)
764 breast cancer. Nat Commun. 2022;13:5258.

765 11. Kudo R, Safonov A, Jones C, Moiso E, Dry JR, Shao H, et al. Long-term breast cancer response
766 to CDK4/6 inhibition defined by TP53-mediated geroconversion. Cancer Cell. 2024;42:1919-1935.

767 12. Zhou Y, Jin X, Ma J, Ding D, Huang Z, Sheng H, et al. HDAC5 Loss Impairs RB Repression
768 of Pro-Oncogenic Genes and Confers CDK4/6 Inhibitor Resistance in Cancer. Cancer Res.
769 2021;81:1486-1499.

770 13. Herrera-Abreu MT, Palafox M, Asghar U, Rivas MA, Cutts RJ, Garcia-Murillas I, et al. Early
771 Adaptation and Acquired Resistance to CDK4/6 Inhibition in Estrogen Receptor-Positive Breast
772 Cancer. Cancer Res. 2016;76:2301–2313.

773 14. Wander SA, Cohen O, Gong X, Johnson GN, Buendia-Buendia JE, Lloyd MR, et al. The
774 Genomic Landscape of Intrinsic and Acquired Resistance to Cyclin-Dependent Kinase 4/6
775 Inhibitors in Patients with Hormone Receptor-Positive Metastatic Breast Cancer. Cancer Discov.
776 2020;10:1174–1193.

777 15. Clark AS, Makhlin I, DeMichele A. Setting the Pick: Can PI3K Inhibitors Circumvent CDK4/6
778 Inhibitor Resistance? Clin Cancer Res. 2021;27:371–373.

779 16. Di Cristofano A, Pandolfi PP, The multiple roles of PTEN in tumor suppression. Cell.
780 2000;100:387–390.

781 17. Song MS, Salmena L, Pandolfi PP. The functions and regulation of the PTEN tumour
782 suppressor. Nat Rev Mol Cell Biol. 2012;13:283–296.

783 18. Lee YR, Chen M, Pandolfi PP. The functions and regulation of the PTEN tumour suppressor:
784 new modes and prospects. Nat Rev Mol Cell Biol. 2018;19:547–562.

785 19. Papa A, Pandolfi PP. The PTEN-PI3K Axis in Cancer. Biomolecules. 2019;9:153.

786 20. Costa C, Wang Y, Ly A, Hosono Y, Murchie E, Walmsley CS, et al. PTEN Loss Mediates
787 Clinical Cross-Resistance to CDK4/6 and PI3Kα Inhibitors in Breast Cancer. Cancer Discov.
788 2020;10:72–85.

789 21. Dosil MA, Mirantes C, Eritja N, Felip I, Navaridas R, Gatius S, et al. Palbociclib has antitumour
790 effects on Pten-deficient endometrial neoplasias. J Pathol. 2017;242:152–164.

791 22. Lee JS, Yost SE, Li SM, Cui Y, Frankel PH, Yuan YC, et al. Genomic Markers of CDK4/6
792 Inhibitor Resistance in Hormone Receptor Positive Metastatic Breast Cancer. Cancers.
793 2022;14:3159.

794 23. Lee YR, Chen M, Lee JD, Zhang J, Lin SY, Fu TM et al. Reactivation of PTEN tumor
795 suppressor for cancer treatment through inhibition of a MYC-WWP1 inhibitory pathway. Science.
796 2019;364:eaau0159.

797 24. Lin YX, Wang Y, Ding J, Jiang A, Wang J, Yu M, et al. Reactivation of the tumor suppressor
798 PTEN by mRNA nanoparticles enhances antitumor immunity in preclinical models. Sci Transl Med.
799 2021;13:eaba9772.

800 25. Kamitani T, Kito K, Nguyen HP, Yeh ET, Characterization of NEDD8, a developmentally
801 down-regulated ubiquitin-like protein. J Biol Chem. 1997;272:28557-62.

802 26. Enchev RI, Schulman BA, Peter M. Protein neddylation: beyond cullin-RING ligases. Nat Rev
803 Mol Cell Biol. 2015;16:30–44.

804 27. Zhang S, Yu Q, Li Z, Zhao Y, Sun Y. Protein neddylation and its role in health and diseases.
805 Signal Transduct Target Ther. 2024;9:85.

806 28. Soucy TA, Smith PG, Milhollen MA, Berger AJ, Gavin JM, Adhikari S, et al. An inhibitor of
807 NEDD8-activating enzyme as a new approach to treat cancer. Nature. 2009;458:732–736.

808 29. Fu DJ, Wang T. Targeting NEDD8-activating enzyme for cancer therapy: developments,
809 clinical trials, challenges and future research directions. J Hematol Oncol. 2023;16:87.

810 30. Xie P, Peng ZQ, Chen YJ, Li HC, Du MG, Tan YW, et al. Neddylation of PTEN regulates its
811 nuclear import and promotes tumor development. Cell Res. 2021;31:291–311.

812 31. Du MG, Peng ZQ, Gai WB, Liu F, Liu W, Chen YJ, et al. The Absence of PTEN in Breast
813 Cancer Is a Driver of MLN4924 Resistance. Front Cell Dev Biol. 2021;9:667435.

814 32. Chakrabarti R, Wei Y, Hang J, Hang X, Andres Blanco M, Choudhury A, et al. ΔNp63 promotes
815 stem cell activity in mammary gland development and basal-like breast cancer by enhancing Fzd7
816 expression and Wnt signalling. Nat Cell Biol. 2014;16:1-13.

817 33. Wan L, Lu X, Yuan S, Wei Y, Guo F, Shen M, et al. MTDH-SND1 interaction is crucial for
818 expansion and activity of tumor-initiating cells in diverse oncogene- and carcinogen-induced
819 mammary tumors. Cancer cell. 2014;26:92-105.

820 34. Guerriero JL, Sotayo A, Ponichtera HE, Castrillon JA, Pourzia AL, Schad S, et al. Class IIa
821 HDAC inhibition reduces breast tumours and metastases through anti-tumour macrophages. Nature.
822 2017;543:428-432.

823 35. Knudsen ES, Knudsen KE. Tailoring to RB: Tumour suppressor status and therapeutic response.
824 Nat Rev Cancer. 2008;8:714–724.

825 36. Guiley KZ, Stevenson JW, Lou K, Barkovich KJ, Kumarasamy V, Wijeratne TU, et al. p27
826 allosterically activates cyclin-dependent kinase 4 and antagonizes palbociclib inhibition. Science.
827 2019;366:6471.

828 37. Eferl R, Wagner EF. AP-1: a double-edged sword in tumorigenesis. Nat Rev Cancer.
829 2003;3:859-868.

830 38. Liu F, Wagner S, Campbell RB, Nickerson JA, Schiffer CA, Ross AH, PTEN enters the nucleus
831 by diffusion. J Cell Biochem. 2005;96:221–234.

832 39. Planchon SM, Waite KAEng, C. The nuclear affairs of PTEN. J Cell Sci. 2008;121:249–253.

833 40. Li Y, Xie P, Lu L, Wang J, Diao L, Liu Z, et al. An integrated bioinformatics platform for
834 investigating the human E3 ubiquitin ligase-substrate interaction network. Nat Commun.
835 2017;8:347.

836 41. Wang X, Li Y, He M, Kong X, Jiang P, Liu X, et al. UbiBrowser 2.0: a comprehensive resource
837 for proteome-wide known and predicted ubiquitin ligase/deubiquitinase-substrate interactions in
838 eukaryotic species. Nucleic Acids Res. 2022;50:D719–D728.

839 42. Van Themsche C, Leblanc V, Parent S, Asselin E, X-linked inhibitor of apoptosis protein (XIAP)
840 regulates PTEN ubiquitination, content, and compartmentalization. J Biol Chem. 2009;284:20462–
841 20466.

842 43. Facino RM, Carini M, Aldini G, Saibene L, Pietta P, Mauri P. Echinacoside and caffeoyl
843 conjugates protect collagen from free radical-induced degradation: a potential use of Echinacea
844 extracts in the prevention of skin photodamage. Planta Med. 1995;61:510–514.

845 44. Wang W, Jiang S, Zhao Y, Zhu G. Echinacoside: A promising active natural products and
846 pharmacological agents. Pharmacol Res. 2023;197:106951.

847 45. Chen BD, Clark CR, Chou TH. Granulocyte/macrophage colony-stimulating factor stimulates
848 monocyte and tissue macrophage proliferation and enhances their responsiveness to macrophage
849 colony-stimulating factor. Blood. 1988;71:997–1002.

850 46. Spiekermann K, Roesler J, Emmendoerffer A, Elsner J, Welte K. Functional features of
851 neutrophils induced by G-CSF and GM-CSF treatment: differential effects and clinical implications.
852 Leukemia. 1997;11:466–478.

853 47. Kolaczkowska E, Kubes P. Neutrophil recruitment and function in health and inflammation.
854 Nat Rev Immunol. 2013;13:159–175.

855 48. Dong F, Guo W, Zhang L, Wu S, Teraishi F, Davis JJ, et al. Downregulation of XIAP and
856 induction of apoptosis by the synthetic cyclin-dependent kinase inhibitor GW8510 in non-small
857 cell lung cancer cells. Cancer Biol Ther. 2006;5:165–170.

858 49. Chen Q, Chen K, Guo G, Li F, Chen C, Wang S, et al. A critical role of CDKN3 in Bcr-Abl-
859 mediated tumorigenesis. PloS One. 2014;9:e111611.

860 50. Burgoyne AM, Vann KR, Joshi S, Morales GA, Vega FM, Singh A, et al. A triple action
861 CDK4/6-PI3K-BET inhibitor with augmented cancer cell cytotoxicity. Cell Discov. 2020;6:49.

862 51. Agostinetto E, Debien V, Marta GN, Lambertini M, Piccart-Gebhart M, de Azambuja E,
863 CDK4/6 and PI3K inhibitors: A new promise for patients with HER2-positive breast cancer. Eur J
864 Clin Invest. 2021;51:e13535.

865 52. Lee CL, Cremona M, Farrelly A, Workman JA, Kennedy S, Aslam R, et al. Preclinical
866 evaluation of the CDK4/6 inhibitor Palbociclib in combination with a PI3K or MEK inhibitor in
867 colorectal cancer. Cancer Biol Ther. 2023;24:2223388.

868 53. Shaulian E, Karin M. AP-1 as a regulator of cell life and death. Nat Cell Biol. 2002;4:E131–
869 E136.

870 54. Ruiz EJ, Lan L, Diefenbacher ME, Riising EM, Da Costa C, Chakraborty A, et al. JunD, not c-
871 Jun, is the AP-1 transcription factor required for Ras-induced lung cancer. JCI Insight.
872 2021;6:e124985.

873 55. Watt AC, Cejas P, DeCristo MJ, Metzger-Filho O, Lam EYN, Qiu X, et al. CDK4/6 inhibition
874 reprograms the breast cancer enhancer landscape by stimulating AP-1 transcriptional activity. Nat
875 cancer. 2021;2:34–48.

876 56. Yamamoto N, Shimizu T, Yonemori K, Kitano S, Kondo S, Iwasa S, et al. A first-in-human,
877 phase 1 study of the NEDD8 activating enzyme E1 inhibitor TAS4464 in patients with advanced
878 solid tumors. Invest New Drugs. 2021;39:1036–1046.

879 57. Zhou H, Lu J, Liu L, Bernard D, Yang CY, Fernandez-Salas E, et al. A potent small-molecule
880 inhibitor of the DCN1-UBC12 interaction that selectively blocks cullin 3 neddylation. Nat Commun.
881 2017;8:1150.

882 58. Zhou H, Zhou W, Zhou B, Liu L, Chern TR, Chinnaswamy K, et al. High-Affinity
883 Peptidomimetic Inhibitors of the DCN1-UBC12 Protein-Protein Interaction. J Med Chem.
884 2018;61:1934–1950.

885 59. Zheng YC, Guo YJ, Wang B, Wang C, Mamun MAA, Gao Y, et al. Targeting neddylation E2s:
886 a novel therapeutic strategy in cancer. J Hematol Oncol. 2021;14:57.

887 60. Xu T, Ma Q, Li Y, Yu Q, Pan P, Zheng Y, et al. A small molecule inhibitor of the UBE2F-
888 CRL5 axis induces apoptosis and radiosensitization in lung cancer. Signal Transduct Target Ther.
889 2022;7:354.

890 61. Liu J, Tang N, Liu N, Lei P, Wang F, Echinacoside inhibits the proliferation, migration, invasion
891 and angiogenesis of ovarian cancer cells through PI3K/AKT pathway. J Mol Histol. 2022;53:493–
892 502.

893 62. Liang H, Yin G, Shi G, Liu Z, Liu X, Li J. Echinacoside regulates PI3K/AKT/HIF-1α/VEGF
894 cross signaling axis in proliferation and apoptosis of breast cancer. Anal Biochem.
895 2024;684:115360.

896 63. Wei J, Zheng Z, Hou X, Jia F, Yuan Y, Yuan F, et al. Echinacoside inhibits colorectal cancer
897 metastasis via modulating the gut microbiota and suppressing the PI3K/AKT signaling pathway. J
898 Ethnopharmacol. 2024;318:116866.

899 64. Giese MA, Hind LE, Huttenlocher A. Neutrophil plasticity in the tumor microenvironment.
900 Blood. 2019;133:2159-2167.

901 65. Teh JLF, Aplin AE. Arrested Developments: CDK4/6 Inhibitor Resistance and Alterations in
902 the Tumor Immune Microenvironment. Clin Cancer Res. 2019;25:921–927.

Figures

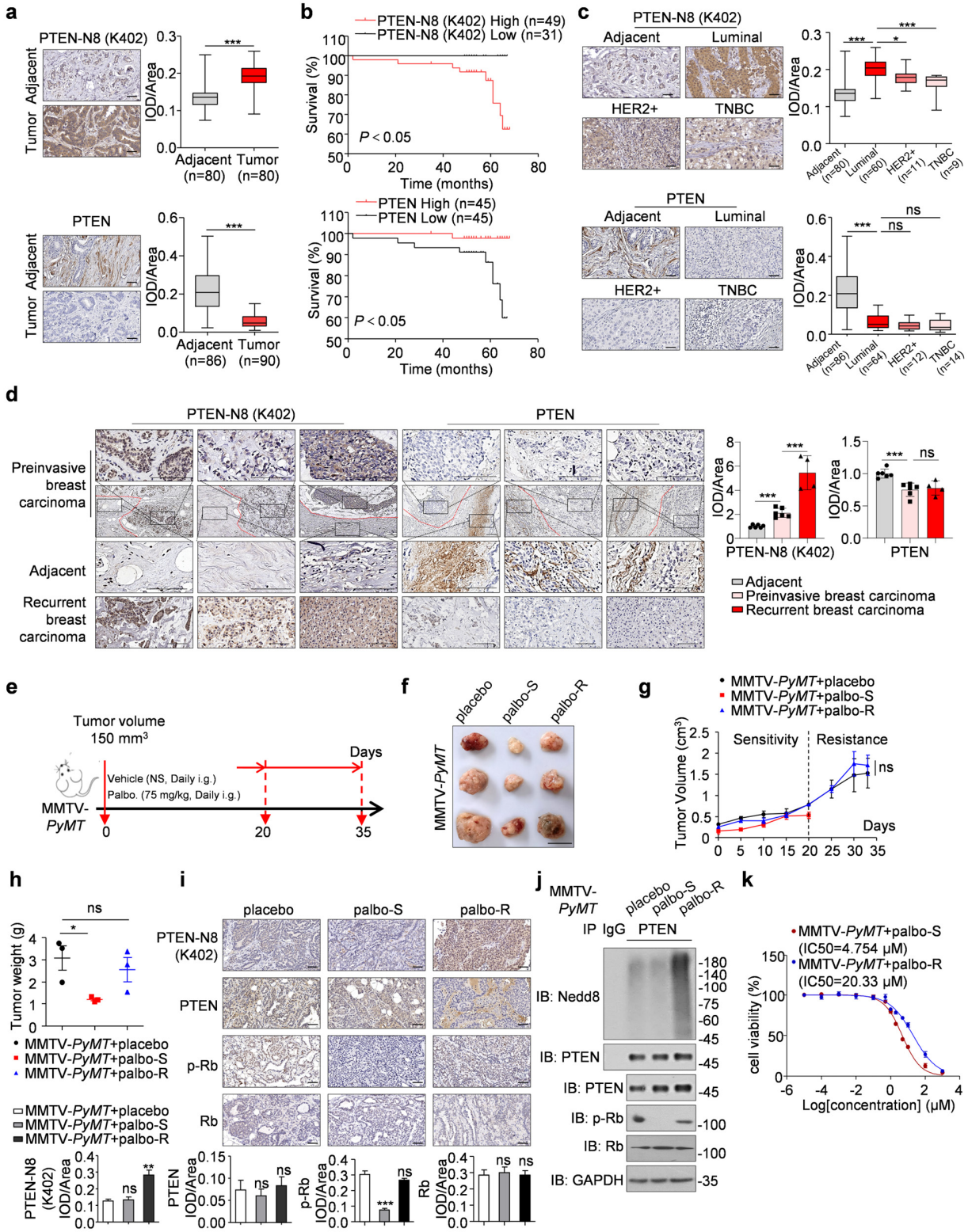

Fig. 1 Palbociclib-resistant breast cancer cells express higher levels of PTEN neddylation modification. **a** Representative images from immunohistochemical staining of PTEN and PTEN

907 neddylation on K402 site in the indicated tissues. Scale bars, 50 μm. **b** Kaplan-Meier plot of overall
908 survival of patients with breast carcinomas. A log-rank test was used to show differences between
909 groups. **c** Representative images from immunohistochemical staining of PTEN and neddylated
910 PTEN on K402 site in different breast cancer subtypes and adjacent tissues are shown. Scale bars,
911 50 μm. PTEN and PTEN neddylation on K402 expression are shown as box plots (a and c). **d**
912 Representative images from immunohistochemical staining of PTEN and PTEN neddylation on
913 K402 in the indicated tissues. Scale bars, 100 μm. The protein level of PTEN and PTEN neddylation
914 on K402 expression are shown as bar plots. **e-h** To establishing the palbociclib-resistant mouse
915 model, the palbociclib-resistant group was established by palbociclib (75 mg/kg) gavage daily for
916 35 days and the palbociclib-sensitive group were administered palbociclib for 20 days (e). The
917 breast tumors were removed and photographed (f). Tumors were isolated, volume (g) and their
918 weights (h) were measured. **i** Representative images from immunohistochemical staining of PTEN,
919 PTEN neddylation on K402, Rb and p-Rb in the indicated groups. Scale bar, 50 μm. **j** Immunoblot
920 analysis of anti-PTEN immunoprecipitate and cell lysates derived from spontaneous breast tumors
921 of MMTV-*PyMT* mice in the indicated groups. **k** IC50 of palbociclib-resistant breast tumor cells
922 obtained from MMTV-*PyMT* mice. The cells were seeded in 96-well plates treated with increasing
923 concentration (0.01 nM-1000 μM) of palbociclib and then analyzed for CCK8 assay. *P* values were
924 calculated by Student's *t*-test. (a and d), log-rank test (b) and one-way ANOVA test (c, g-i). Error
925 bars, ± S.D. ns, not significant, $*P < 0.05$, $**P < 0.01$, $***P < 0.001$.

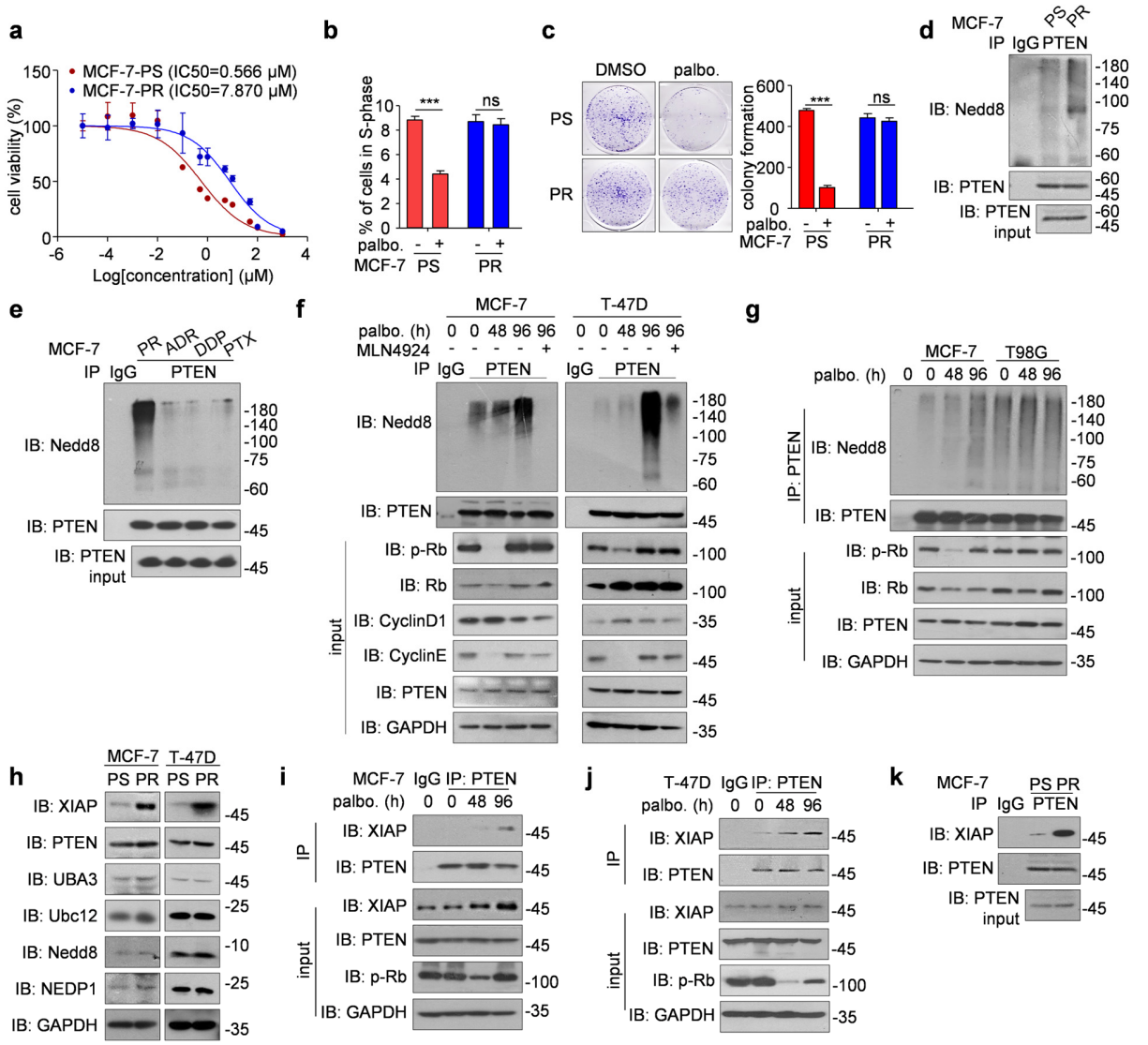

Fig. 2 Upregulation of XIAP increases the PTEN neddylation in palbociclib-resistant breast cancer. **a** IC50 of MCF-7-PS (palbociclib sensitivity, PS) and MCF-7-PR (palbociclib resistance, PR) cells. MCF-7-PR cells and MCF-7-PS cells were seeded in 96-well plates and then treated with increasing concentrations (0.01 nM-1000 μM) of palbociclib and then ananlyzed for CCK8 assay. **b** MCF-7-PS and MCF-7-PR cells are treated with palbociclib (0.5 μM, 24 h). The percentage of cells in G1/S-phase is depicted. **c** Colony formation assay was performed in the MCF-7-PS cells and MCF-7-PR cells and the cells were treated with palbociclib (0.1 μM, 15 days). Results are from a representative experiment performed in triplicate. **d** Immunoblot analysis of anti-PTEN immunoprecipitate from MCF-7-PS and MCF-7-PR cells to detect PTEN neddylation *in vivo*. **e**

936 Immunoblot analysis of anti-PTEN immunoprecipitate from MCF-7 drug resistant cells including
937 MCF-7-PR, MCF-7 sublines resistant to doxorubicin (MCF-7-ADR), cisplatin (MCF-7-DDP) and
938 paclitaxel (MCF-7-PTX) cells. **f** MCF-7 cells and T-47D cells were treated with palbociclib (0.5
939 μM, 0 h/48 h/96 h). The right pannel was treated with palbociclib (0.5 μM, 96 h) and MLN4924 (1
940 μM, 12 h) simultaneously. The cells were collected and lysed for immunoblot analysis with
941 indicated antibodies. **g** Immunoblot analysis of anti-PTEN immunoprecipitate from MCF-7 cells
942 and T98G cells. MCF-7 cells and T98G cells were respectively treated with palbociclib (0.5 μM, 0
943 h/48 h/96 h). **h** Western blot analysis of XIAP, PTEN, UBA3, Ubc12, Nedd8, NEDP1 in palbociclib
944 sensitivity and resistance MCF-7 and T-47D cells. **i** and **j** Immunoblot analysis of anti-PTEN
945 immunoprecipitate and WCL from adaptative palbociclib resistance in MCF-7 (i) and T-47D (j). **k**
946 Co-immunoprecipitation of XIAP after immunoprecipitation of the PTEN protein in palbociclib
947 sensitivity and resistance MCF-7 cells. *P* values were calculated by one-way ANOVA test (a and c).
948 Error bars, ± S.D. ns, not significant, ***$P < 0.001$.

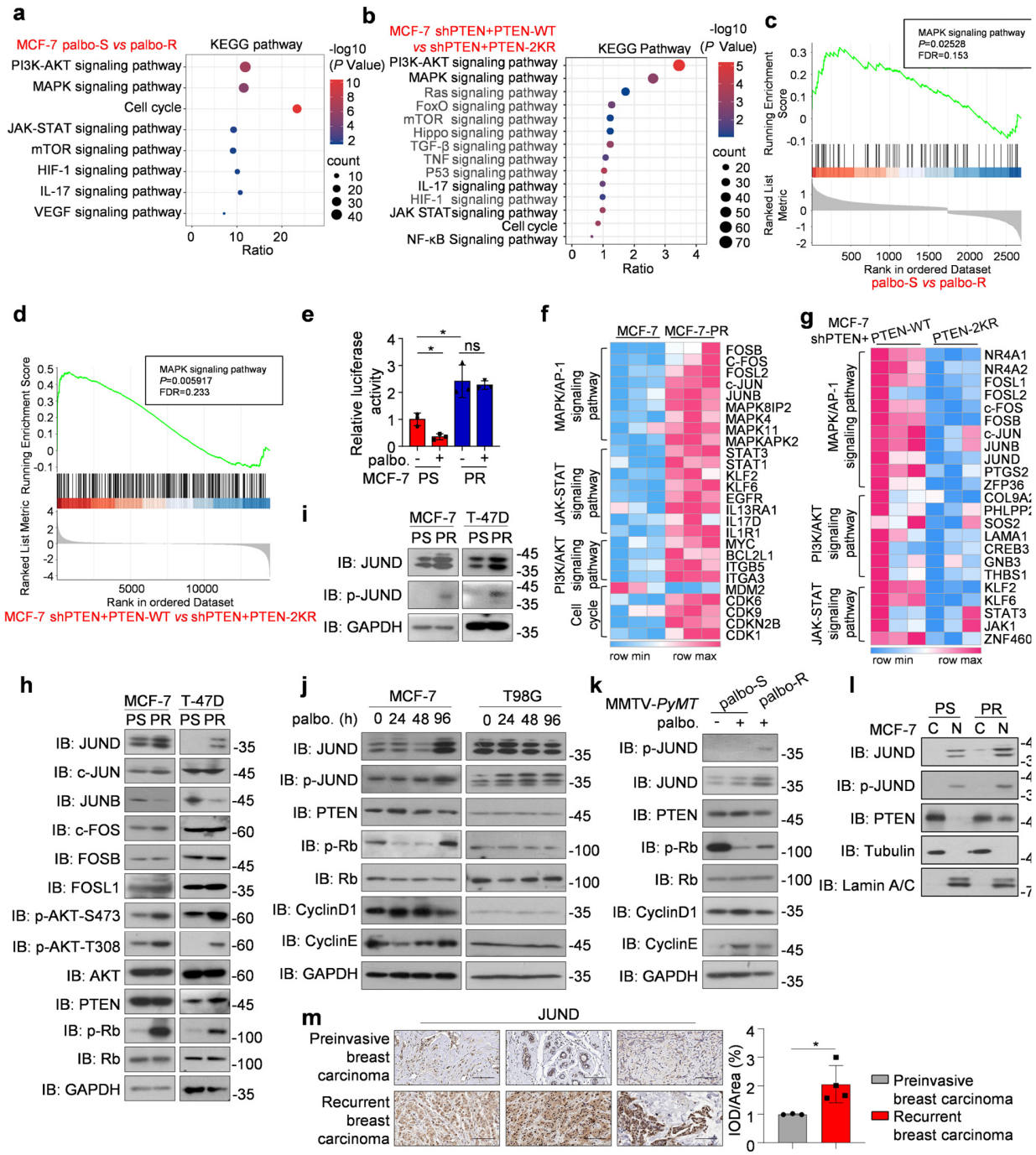

Fig. 3 PTEN neddylation enhances JUND protein stability. **a** and **b** The bubble charts depict the top ranked pathway analyzed from the KEGG pathway database. Enriched KEGG pathways were identified, which included upregulated or downregulated genes modulated by the palbociclib resistance MCF-7 cells (a) and MCF-7 cells harboring a PTEN neddylation mutation (b). **c** and **d** GSEA plots of the palbociclib resistance MCF-7 cells (c) and PTEN neddylation deficiency MCF-

955 7 cells (d). **e** AP-1 luciferase reporter plasmid was transfected in the palbociclib sensitivity and
956 resistance MCF-7 cells. Reporter activity was assayed and represented as the means ± S.D. of three
957 separate experiments. **f** and **g** Heat map of the palbociclib resistance MCF-7 cells (f) and PTEN
958 neddylation deficiency MCF-7 cells (g). **h** and **i** Immunoblot of WCL from acquired palbociclib-
959 sensitive or palbociclib-resistant cells. **j** Western blot analysis of lysates from MCF-7 cells treated
960 for 24 to 96 hours with palbociclib (palbo). Addition of fresh vehicle or drug every 24 hours over a
961 96-hour period. **k** The cells obtained from breast tumors of MMTV-*PyMT* mice were collected and
962 lysed for immunoblot analysis. **l** Immunoblot of Nuclear (N) *vs* Cytoplasmic (C) fractionation from
963 palbociclib sensitivity and resistance MCF-7 cells. **m** Representative images from
964 immunohistochemical staining of JUND in palbociclib-resistant breast tumors and matched
965 adjacent tissues. ImageJ was used to perform Semi-quantitative analysis. Scale bars, 50 μm. *P*
966 values were calculated by Student's *t*-test. Error bars, ± S.D. ns, not significant, *$P < 0.05$, **$P <$
967 0.01, ***$P < 0.001$.

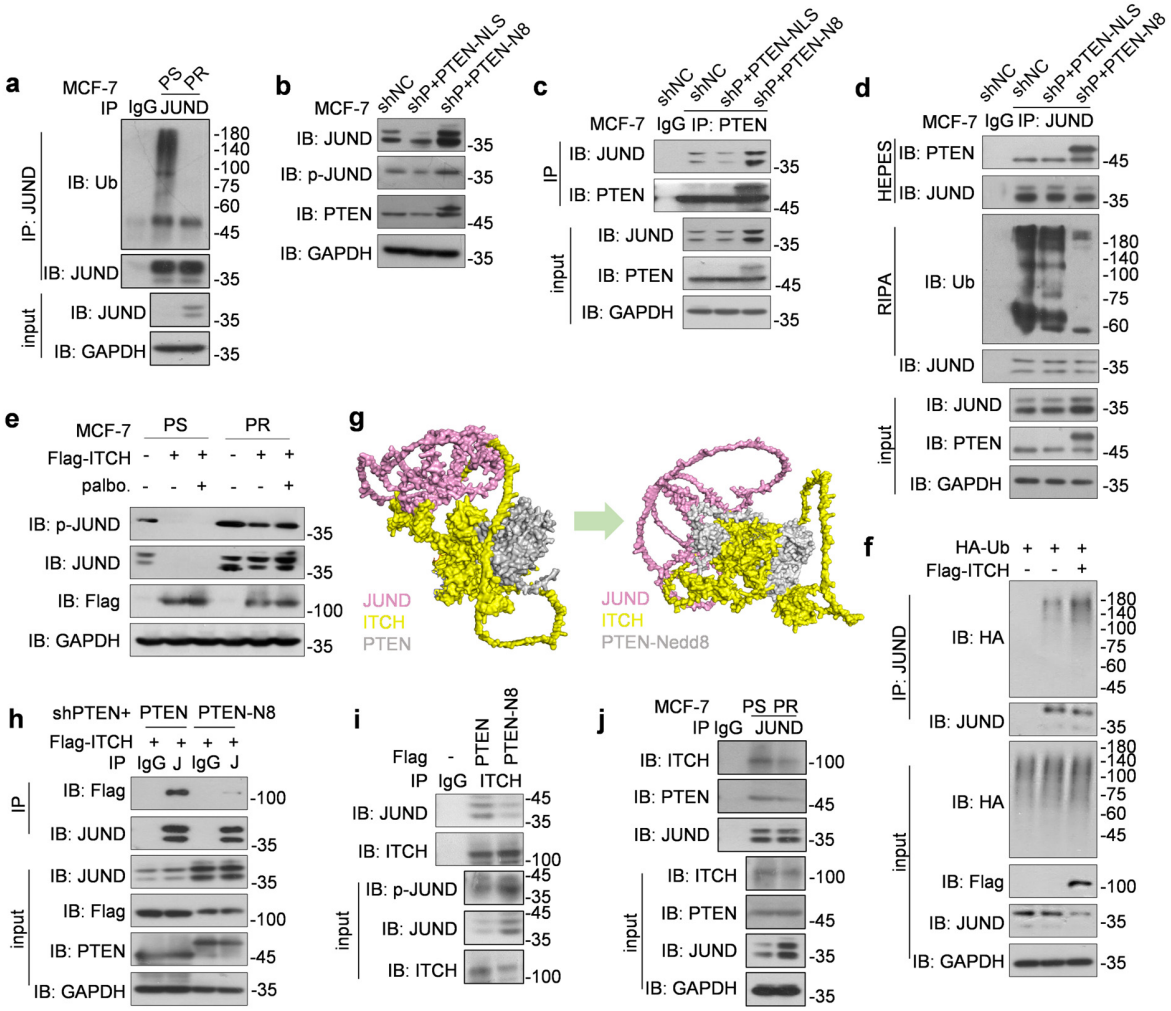

Fig. 4 PTEN neddylation hinders the ITCH-mediated ubiquitination degradation of JUND. **a** Immunoprecipitation of JUND in the MCF-7-PS and MCF-7-PR cells and analysis using immunoblotting with the indicated antibodies. **b** Immunoblot of JUND and p-JUND in the MCF-7 sh*NC*, MCF-7 sh*PTEN*+PTEN-NLS and MCF-7 sh*PTEN*+PTEN-N8 cells. **c** and **d** Immunoprecipitation of PTEN (c) and JUND (d) in the MCF-7 sh*NC*, MCF-7 sh*PTEN*+PTEN-NLS and MCF-7 sh*PTEN*+PTEN-N8 cells. **e** Flag tagged-ITCH was transfected into the MCF-7-PS cells and MCF-7-PR cells and immunoblotted with the indicated antibodies. The cells were treated with palbociclib (0.5 μM for 48 h). **f** Immunoprecipitation of JUND in HEK293T cells transfected with plasmids of HA-tagged-Ub, Flag-tagged-ITCH and analysis using immunoblot analysis with the indicated antibodies. **g** Structure simulation of ITCH (yellow), JUND (pink) and

979 PTEN or PTEN-Nedd8 (grey) by AlphaFold2.0. **h** MCF-7 sh*PTEN*+PTEN-WT and MCF-7
980 sh*PTEN*+PTEN-N8 cells transfected with plasmids for Flag-tagged ITCH and analyzed using
981 immunoblot analysis with the indicated antibodies. **i** Flag tagged-PTEN or PTEN-Nedd8 plasmid
982 was transfected into the MCF-7 cells and immunoblotted with the indicated antibodies. **j** Co-
983 immunoprecipitation of ITCH and PTEN after immunoprecipitation of the JUND protein in
984 palbociclib sensitivity and resistance MCF-7 cells.

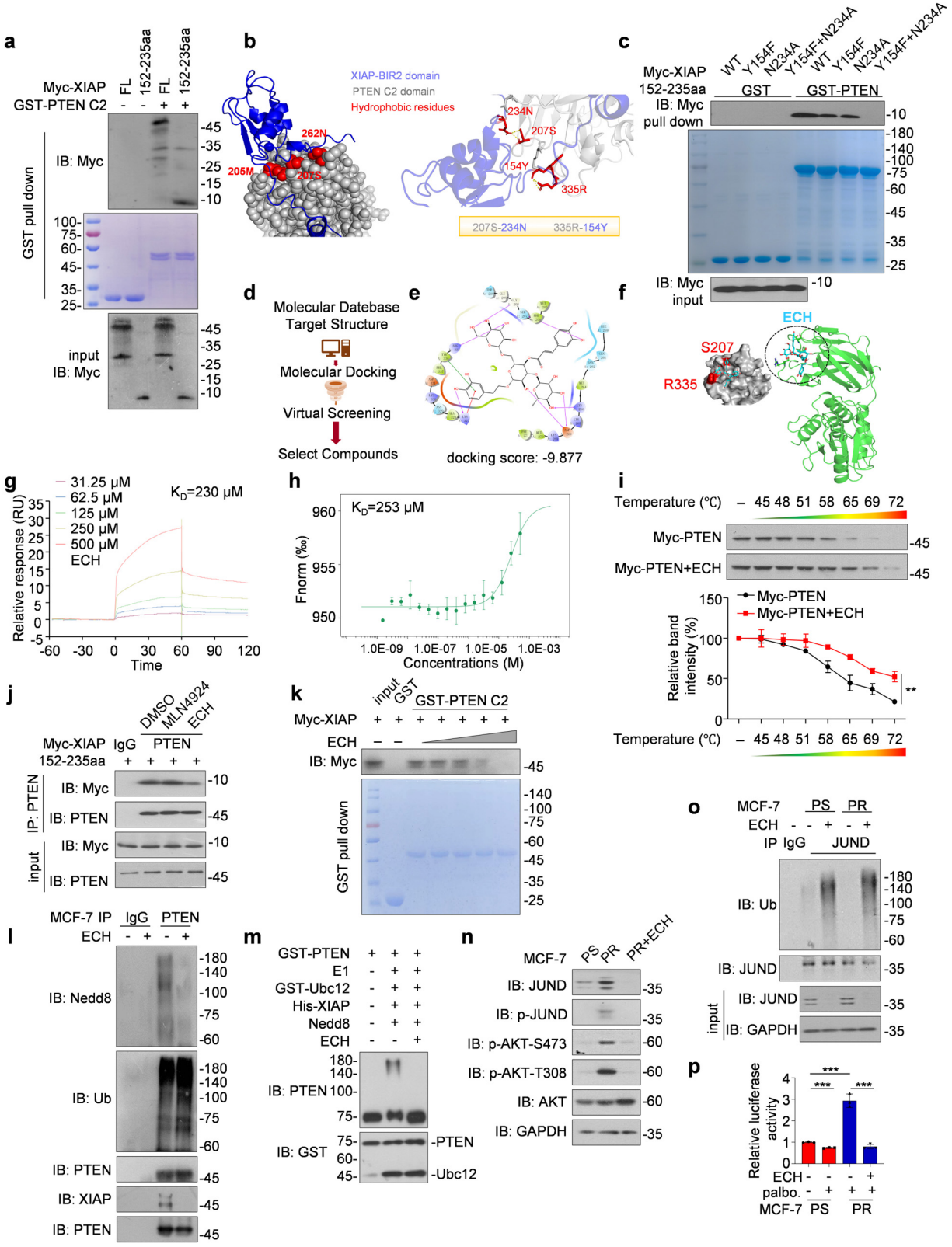

Fig. 5 Echinacoside is identified as an inhibitor of PTEN neddylation. **a** and **c** Immunoblot analysis of GST pull-downs or WCL from HEK293T cells transfected with indicated constructs. **b**

988 Molecular docking of PTEN C2 domain (gray) and XIAP BIR2 domain (blue). **d** The workflow of
989 virtual drug screening. **e** Structural formula and molecular docking score of Echinacoside with
990 PTEN. **f** Molecular docking of Echinacoside (ECH) with PTEN was conducted to estimate the
991 binding affinity. **g** Representative images of SPR binding assay of ECH to PTEN. ECH exhibited
992 dose-dependent binding to GST-tagged PTEN that was immobilized onto a CM5 sensor chip
993 surface. **h** All hits were titrated at various serially diluted concentrations (0.0153 μM to 500 μM)
994 into a fixed concentration of GST-PTEN C2 domain (150 nM). **i** Dose and temperature-dependent
995 CETSA experiments were conducted to verify the interaction between Echinacoside (ECH) and
996 PTEN. **j** Immunoprecipitates of PTEN were obtained from HEK293T cells transfected with Myc-
997 XIAP (amino acids 152-235) and treated with either MLN4924 (0.5 μM) and Echinacoside (ECH)
998 (200 μM) for 24 h. **k** Immunoblot analysis of GST pull-downs or WCL from HEK293T cells
999 transfected with indicated constructs. The concentration of ECH was used from 20 μM to 200 μM
1000 for 24 h. **l** PTEN neddylation was attenuated by ECH *in vivo*. Immunoblot analysis of anti-PTEN
1001 immunoprecipitate and WCL from indicated cells. **m** *In vitro* neddylation of PTEN. Reactions were
1002 performed as described in the materials and methods section. ECH (100 μg) was added and reacted
1003 for 1 h. **n** Immunoblot of WCL from MCF-7 PS and PR cells for indicated proteins. **o** *In vivo*
1004 ubiquitination of PTEN. Immunoblot analysis of anti-JUND immunoprecipitate and WCL from
1005 indicated cells. **p** AP-1 luciferase reporter plasmid was transfected in indicated cells. Reporter
1006 activity was assayed in the indicated cells.

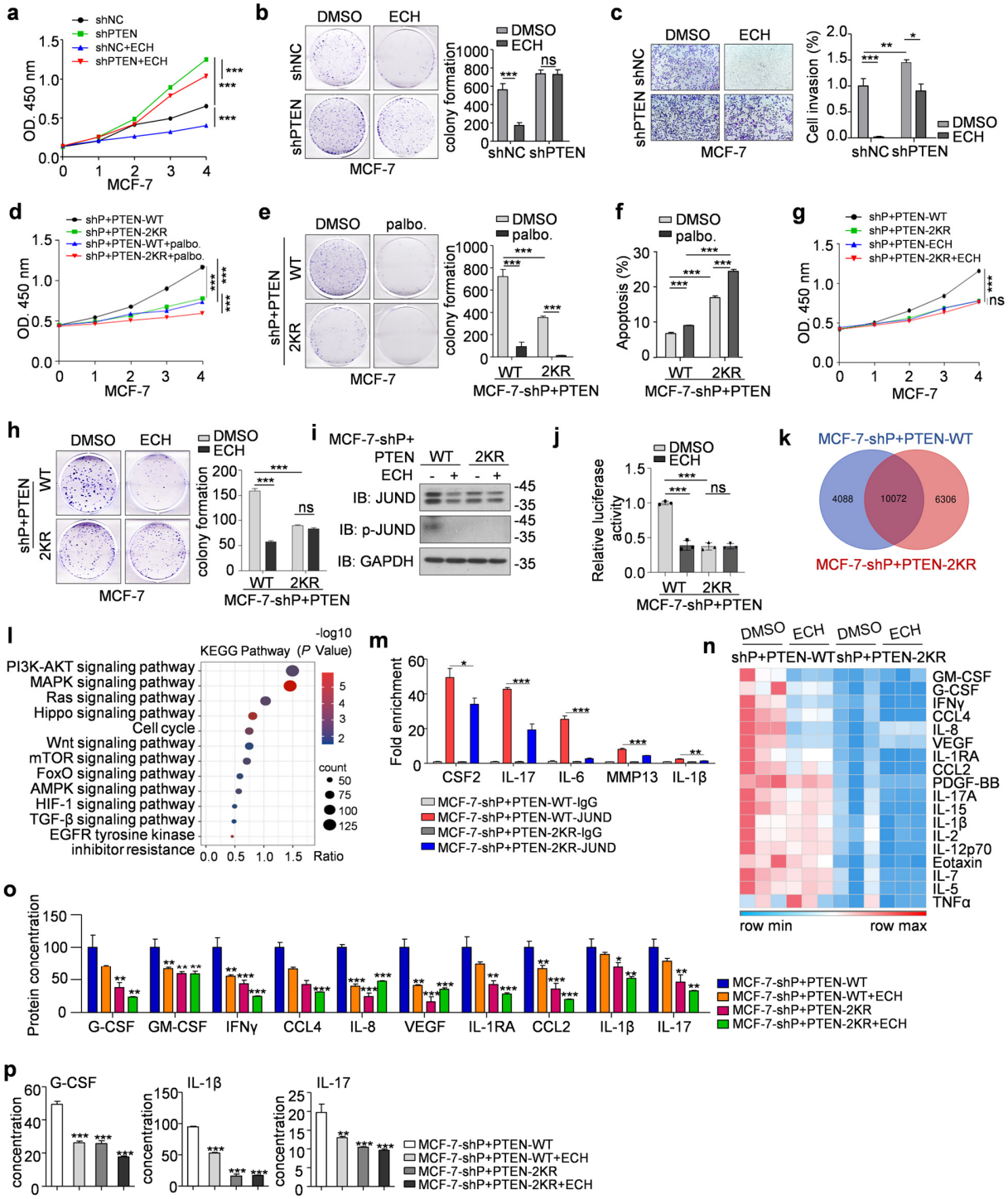

Fig. 6 ECH is dependent on PTEN neddylation to suppress tumorigenesis. **a-c** CCK8 (a), colony formation (b) and cell invasion assay (c) were performed in the indicated MCF-7 cells treated with ECH. **d-f** CCK8 (d), colony formation (e) and apoptosis assay (f) were performed in the indicated MCF-7 cells treated with palbociclib. **g** and **h** CCK8 (g), and colony formation (h) were performed

1012 in the indicated MCF-7 cells treated with ECH. **i** Immunoblot of WCL from the sh*PTEN*+PTEN-
1013 WT/2KR MCF-7 cells treated by ECH (200 μM, 24 h). **j** AP-1 luciferase reporter plasmid was
1014 transfected in the indicated cells. Reporter activity was assayed in the cells treated with ECH (200
1015 μM) for 24 h. **k** and **l** Identification of transcription targets of the JUND in the sh*PTEN*-PTEN WT
1016 or neddylation deficient MCF-7 cells. Venn diagrams of overlapped promoters bound by JUND (k).
1017 A bubble chart of the enriched KEGG pathways comprising the 6306 target genes (l). **m** qChIP
1018 analysis of the indicated genes in indicated MCF-7 cells. Results are represented as fold change
1019 relative to control with GAPDH as a negative control. **n** Cytometric bead array was performed to
1020 detect the indicated cytokines. Heat map was performed to exhibit protein expression in the
1021 indicated cells. The cells were treated with ECH (200 μM) for 24 h. **o** The protein level of G-CSF,
1022 GM-CSF, IFNγ, CCL2, IL-8, VEGF, IL-1RA, IL-1β, IL-17 and CCL4 from the immunoassay array
1023 of the indicated MCF-7 cells are shown as bar chart. **p** G-CSF，IL-1β and IL-17 protein levels
1024 were measured in the indicated MCF-7 cells by ELISA assay. *P* values were calculated by one-way
1025 ANOVA test (a-h, j, m, o, p). Error bars, ± S.D. ns, not significant, **P* < 0.05, ***P* < 0.01, ****P* <
1026 0.001.

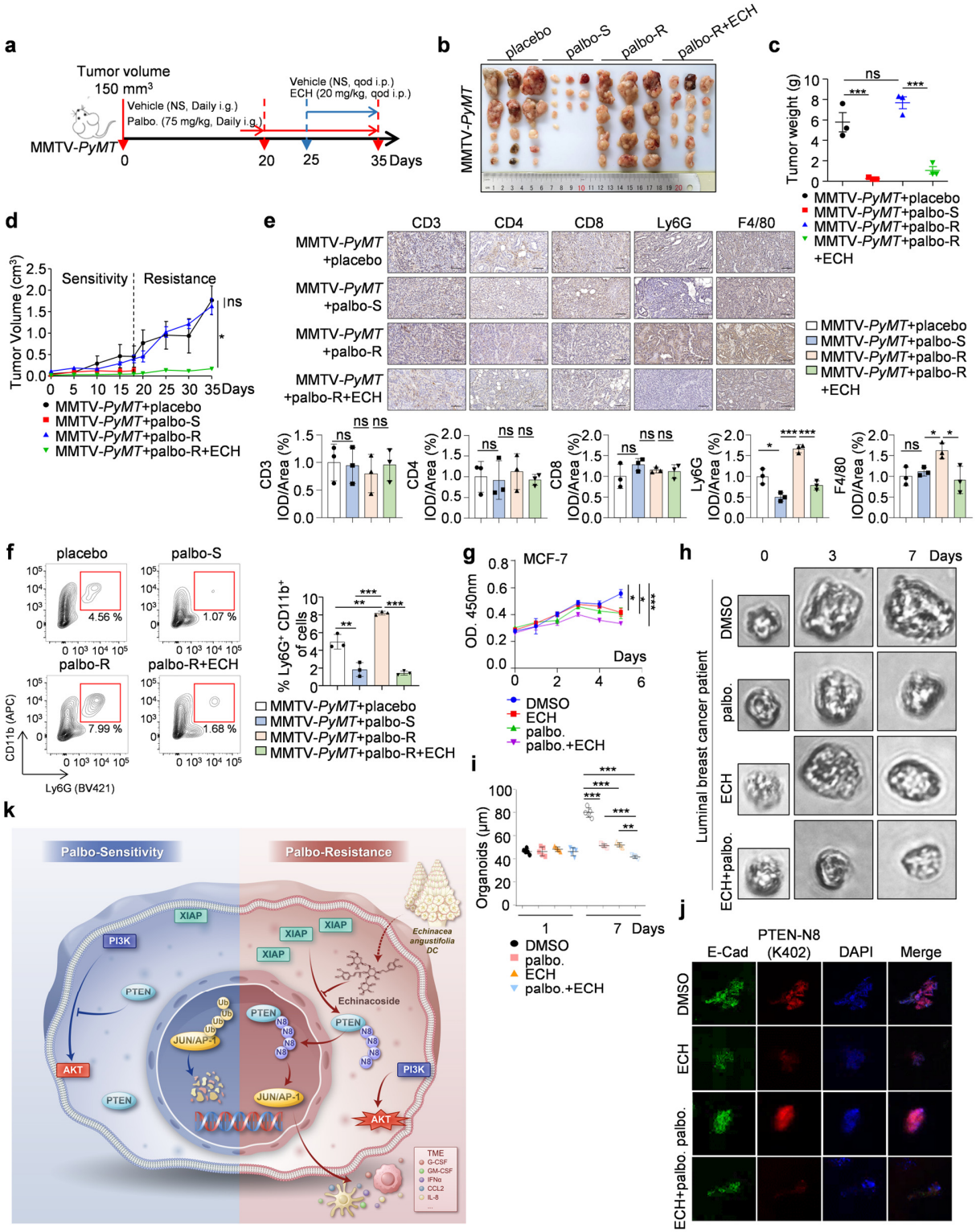

Fig. 7 Combination ECH enhances the sensitivity of palbociclib in breast cancer. **a-d** The palbociclib-resistant mice model (n=3) was established (a). The mice were treated with ECH (20 mg/kg) for 10 days. The breast tumors were removed and photographed (b). Tumors were isolated,

1031 then the weights (c) and their volume (d) were measured. Data are presented as means ± S.D. **e**
1032 Representative images from immunohistochemical staining of CD3, CD4, CD8, Ly6G and F4/80
1033 in the indicated tumors. ImageJ was used to perform Semi-quantitative analysis. Scale bars, 50 μm.
1034 **f** Primary breast cancer cells from the indicated MMTV-*PyMT* mice were isolated and labeled with
1035 $CD11b^+$ and $Ly6G^+$ following flow cytometry sorting. **g** CCK8 assay was performed in MCF-7
1036 cells treated with palbociclib (0.5 μM, 5 days) and ECH (200 μM, 5 days). **h** and **i** Representative
1037 images of organoids derived from a luminal breast cancer patient (h). Echinacoside (ECH) (200
1038 μM) and palbociclib (0.5 μM) were administered either individually or in combination for 7 days.
1039 The diameters of the organoids are presented as a scatter plot (i). **j** Immunofluorescent of E-
1040 Cadherin (green) and neddylated PTEN (K402) (red) in luminal breast cancer organoids. **k** Working
1041 model for PTEN neddylation aggravates CDK4/6 inhibitor resistance in breast cancer. Data are
1042 shown as means ± S.D. and analyzed by a one-way ANOVA test (c-g, i). ns, not significant, *$P <$
1043 0.05, **$P < 0.01$, ***$P < 0.001$.